Neuroimaging of Pediatric Brain Tumors: From Basic to Advanced Magnetic Resonance Imaging (MRI)

Ashok Panigrahy and Stefan Blüml

J Child Neurol 2009 24: 1343
DOI: 10.1177/0883073809342129

Special Issue Article

Journal of Child Neurology
Volume 24 Number 11
November 2009 1343-1365
© 2009 The Author(s)
10.1177/0883073809342129
http://jcn.sagepub.com

Neuroimaging of Pediatric Brain Tumors: From Basic to Advanced Magnetic Resonance Imaging (MRI)

Ashok Panigrahy, MD, and Stefan Blüml, PhD

In this review, the basic magnetic resonance concepts used in the imaging approach of a pediatric brain tumor are described with respect to different factors including understanding the significance of the patient's age. Also discussed are other factors directly related to the magnetic resonance scan itself including evaluating the location of the tumor, determining if the lesion is extra-axial or intra-axial, and evaluating the contrast characteristics of the lesion. Of note, there are key imaging features of pediatric brain tumors, which can give information about the cellularity of the lesion, which can then be confirmed with advanced magnetic resonance imaging (MRI) techniques. The second part of this review will provide an overview of the major advanced MRI techniques used in pediatric imaging, particularly, magnetic resonance diffusion, magnetic resonance spectroscopy, and magnetic resonance perfusion. The last part of the review will provide more specific information about the use of advanced magnetic resonance techniques in the evaluation of pediatric brain tumors.

Keywords: advanced MR imaging; brain tumors; MRI; CT scan

Pediatric brain tumors are the second most frequent malignancy of childhood, exceeded only by leukemia, and the most common form of solid tumor. There are approximately 2500 new diagnoses per year in the United States, and the incidence of brain tumors has increased slightly over the decades. Brain tumors comprise 20% to 25% of all malignancies occurring among children under 15 years of age and 10% of tumors occurring among 15- to 19-year-old children. Brain tumors are the leading cause of death from cancer in pediatric oncology. In addition, survivors of childhood brain tumors often have severe neurological, neurocognitive, and psychosocial sequelae due to either the effects of the tumor or the treatment required to control it. Among brain tumor participants, approximately 35% of all patients are younger than 5 years and 75% are younger than 10 years. The type of tumors, the overall incidence of brain tumors, and the risks of poor outcome change with the age. Young children are at the highest risk because tumors tend to be more malignant in their behavior in this age group. Childhood brain tumors display a high pathologic heterogeneity. Whereas most brain tumors in adults are gliomas (≈70% malignant anaplastic astrocytoma and glioblastoma), a significant portion of pediatric brain tumors are other tumor types such as medulloblastoma, pilocytic astrocytomas, ependymomas, and others (Table 1). Genetic risk factors for brain tumors include neurofibromatosis types 1 and 2 (pilocytic astrocytoma, low-grade gliomas, and ependymoma), Turcot syndrome (medulloblastoma and high-grade glioma), Li-Fraumeni syndrome, Gorlin syndrome, and von Hippel-Lindau syndrome (hemangioblastoma).

Basic Differences Between Computed Tomography and Magnetic Resonance Imaging

Usually the first imaging study of a pediatric patient with a brain tumor is computed tomography ([CT] roentgen-ray computed tomography) imaging. With CT imaging, a beam of x-rays is shot straight through the brain. As it

Received June 15, 2009. Accepted for publication June 15, 2009.

From the Department of Radiology, Childrens Hospital Los Angeles, Los Angeles, California.

We acknowledge our multidisciplinary neuro-oncology team at CHLA including the neuro-oncologists (including Drs Finlay, Dhall, Epstein, Villablanca, and Jubran), the neurosurgeons (Drs Krieger and McComb), neuroradiologist (Drs Nelson and Jackson), the neurologists (Drs Mitchell and Rosser), neuropathologist (Drs Gonzalez and Gilles), and nurse practioners (including Barbara Britt) for their excellent world class care of children with brain tumors. We acknowledge the organizations that support our research including the National Institutes of Health, the Thrasher Research Fund, Ian's Friends Foundation, and Rudi Schulte Research Institute. We also acknowledge Julia Castro for editorial assistance.

Address correspondence to: Ashok Panigrahy, Department of Radiology, Childrens Hospital Los Angeles, 4650 Sunset Blvd, MS 81, Los Angeles, CA 90027; e-mail: apanigrahy@chla.usc.edu.

Panigrahy A, Blüml S. Neuroimaging of pediatric brain tumors: from basic to advanced Magnetic Resonance Imaging (MRI). *J Child Neurol.* 2009;24:1343-1365.

Table 1. World Health Organization Grade and Approximate Relative Incidence of the Most Common Pediatric Brain Tumors[a]

Diagnosis	World Health Organization Grade[b]	Location	Relative Frequency
Medulloblastoma	4	Posterior fossa	≈20%
Pilocytic astrocytoma	1	Posterior fossa, hypothalamic/third ventricular region, optic nerve, and chiasmal region	≈20%
Astrocytoma		Anywhere in the brain	≈20%-25%
Low-grade astrocytoma	2		
Anaplastic astrocytoma	3		
Glioblastoma	4		
Ependymal tumors		Mostly posterior fossa	≈10%-15%
Ependymoma	2		
Anaplastic ependymoma	3		
Choroid plexus tumors		Mostly intraventricular, growing out from choroid plexus tissue	≈3%
Papilloma	1		
Carcinoma	3		
Germ cell tumors		Pineal and suprasellar regions, also basal ganglia	≈3%
Pure germinomas			
Mixed germ cell tumors			
Craniopharyngioma	1	Sellar region, not a primary brain tumor	≈4%
Other			≈5%-10%
Neuronal and mixed neuronal-glial tumors, etc			

a. Among the more than 100 subtypes of pediatric brain tumors, medulloblastoma, pilocytic astrocytomas, astrocytomas, and ependymomas constitute more than 80%. Note that the incidence of individual tumors changes with age.
b. The 2007 World Health Organization classification of tumors of the central nervous system.

comes out the other side, the beam is blunted slightly because it hits dense living tissues on the way through. Blunting or "attenuation" of the x-ray comes from the density of the tissue encountered along the way. Very dense tissue like bone or calcification blocks a relatively higher number of x-rays; gray matter blocks some and fluid relatively less. This allows different densities or attenuations to be created in the brain x-ray detectors positioned around the circumference of the scanners collecting attenuation readings from multiple angles. A computerized algorithm reconstructs an image of each slice. The advantage of CT imaging is that it is widely available and as a result is usually the first imaging study which is performed when a pediatric patient first presents with neurological symptoms that may be related to pediatric brain tumor.

With magnetic resonance imaging (MRI), protons are placed in a magnetic field and they become capable of receiving and then transmitting electromagnetic energy. The strength of the transmitted energy is proportional to the number of protons in the tissue. Signal strength is modified by the properties of each proton's microenvironment, such as its mobility and the local homogeneity of the magnetic field. Magnetic resonance signal can be "weighted" to accentuate some properties and not others. T1 signal is used mostly for anatomic imaging, evaluating blood products, and contrast imaging. T2 imaging is used to evaluate edema. Fluid attenuated inversion recovery is a sequence that significantly improves the conspicuity of the edema. When an additional magnetic field is superimposed, one which is carefully varied in strength at different points in space, each point in space has a unique radio frequency at which the signal is received and transmitted. The advantage of magnetic resonance over CT is the lack of radiation exposure. However, younger pediatric patients with brain tumors usually need to be sedated for magnetic resonance. Standard anatomical pre- and post-contrast MRI is the method of choice to determine tumor size, location, and the status of the blood–brain barrier. This information is often sufficient for diagnosing the tumor type and for making immediate treatment decisions.[1-3] Conventional MRI is also essential for assessing the impact of therapy by determining the completeness of resection, monitoring the size of lesions, and detecting recurrent disease.

Basic Magnetic Resonance Concepts in Pediatric Brain Tumors

Multiple factors are considered to render an accurate differential in the diagnosis of a pediatric brain tumor including the age, location, intra-axial versus extra-axial location, the cellularity of the lesion (T2 signal and apparent diffusion coefficient values), enhancement characteristics, and the amount of perilesional edema as determined by fluid attenuated inversion recovery imaging.

In general, intra-axial lesions narrow the cerebrospinal fluid space and displace the cortex toward the periphery. In contrast, extra-axial lesions tend to widen the cerebrospinal fluid spaces and displace the brain deeper, and the lesion has a broad base toward the dura. The locations and the differential diagnosis of both intra-axial and extra-axial lesions are listed in Table 2.

Table 2. Intra-Axial vs Extra-Axial of Brain Tumors

Intra-Axial		Extra-Axial	
Location	Differential	Location	Differential
Cortex	Glioma	Subarachnoid	Meningioma
Gray–White junction	Medulloblastoma	Subdural	Pituitary adenoma
Deep white matter	Hemangioblastoma	Epidural	Craniopharyngioma
Intraventricular	Metastases	Calvarium	Schwannoma
	Infaction/hematoma	Subgaleal	Chordoma
	AVM/congenital	Scalp (soft tissue)	Dermoid/epidermoid, cyst, lipoma
	Abscess/inflammation		Hematoma, metastasis, infection

Note: AVM, arteriovenous malformation.

Table 3. Supratentorial and Infratentorial Locations of Neonatal Brain Tumors[a]

	Presentation at Birth		Presentation in First 2 Months	
	Supratentorial	Infratetorial	Supratentoria	Infratentorial
Teratoma	44	0	18	1
Neuroepithelial				
Medulloblastoma	2	7	1	8
Astrocytoma	5	3	9	2
Choroid plexus papilloma	6	0	9	0
Ependymoma, ependymoblastoma	4	0	7	2
Other neuroepithelial	10	6	8	2
Total of all neuroepithelial tumors	27	16	34	14

a. Adapted from Wakai S, Arai T, Nagai M: *Surg Neurol*. 23:597-609, 1984.

Contrast enhancement in conventional MRI represents a pathologic alteration of the blood–brain barrier. Normal areas of contrast enhancement in the brain occur in the choroids plexus, the pineal gland, and the pituitary gland. Different locations of enhancement include leptomeningeal (pial), pachymeningeal (dural), and ependymal tissue. The morphology of contrast enhancement includes homogeneous, heterogeneous, ring, or serpentine. A neoplastic process may destroy capillaries that can result in contrast enhancement. However, contrast enhancement may also result from the development of newly formed abnormal capillaries. The degree of enhancement does not generally correlate with tumor grade as benign lesions like pilocytic astrocytomas or low-grade choroid plexus papilloma can enhance whereas malignant anaplastic astrocytoma often do not present with contrast agent accumulation.

Perilesional edema is best evaluated with the use of fluid attenuated inversion recovery sequences. The general belief is that fast growing and invasive lesions incite a greater vasogenic edema response than slow growing tumors. In some neoplasms, the perilesional edema may be a combination of both vasogenic edema and tumoral edema.

Age Distribution of Lesion

Neonatal Brain Tumors

The most common congenital brain tumor is the teratoma. It is usually found in the midline regions and has heterogeneous characteristics including components of fat and calcifications. The second most common tumor type at birth is the neuroepithelial tumors that comprise medulloblastoma, astrocytomas, ependymomas, and choroid plexus tumors. After 2 months of life, the neuroepithelial tumors are more common than teratoma (Table 3). During this time period, supratentorial lesions are more common than infratentorial lesions.

Table 4. Brain Tumors in Children Less Than 2 Years of Age

Two thirds are supratentorial
Most common tumors
Primitive neuroectodermal tumor (PNET)
Astrocytoma
Teratoma
Choroid plexus papilloma

Tumors in Pediatric Patients Less Than 2 Years of Age

In these infants, most of the lesions are supratentorial. Neuroepithelial tumors are the most common tumor type in this age range (Table 4).

Tumors in Pediatric Patients Greater Than 2 Years of Age

In pediatric patients greater than 2 years of age, the number of infratentorial tumors slightly exceeds supratentorial

Table 5. Brain Tumors in Children

52% supratentorial
Just under half are cerebral hemisphere,astrocytomas (mostly low grade), craniopharyngiomas, opticochiasmatic-hypothalamic gliomas
Remainder
Pineal region tumors (germinoma, pineal, parenchymal cell tumors)
Primitive neuroectodermal tumor
Choroid plexus papilloma
Others (ganglioglioma, oligodendroglioma, dysembryoplastic neuroepithelial tumors)
48% infratentorial
Cerebellar astrocytomas, brain stem astrocytomas, medulloblastoma (primitive neuroectodermal tumor–medulloblastoma), ependymomas

tumors. The infratentorial lesions tend to be comprised of pilocytic astrocytomas, medulloblastoma, ependymoma, and brain stem tumors. These lesions can also occur in the supratentorial regions (Table 5).

Location of Tumors

Posterior Fossa Lesions

The main candidates for posterior fossa lesions in the pediatric patient are medulloblastomas, ependymomas, and pilocytic astrocytomas. Medulloblastomas tend to arise from the roof of the fourth ventricle and the inferior medullary velum (Figure 1). They tend to have hypointense T2 signal corresponding with the increased cellularity of the lesion. Ependymomas tend to arise from the floor of the fourth ventricle and then extend through the foramen of Luschka or Magendie (Figure 1). Pilocytic astroctyomas tend to be cystic with a mural nodule (Figure 2). The solid portion of the lesion is usually hyperintense on T2 imaging, correlating with the hypocellular nature of the lesion (Figure 2). Pilocytic lesions can present as more solid lesions in certain cases (Figure 2). Ependymomas can have varied T2 signal depending on the histological subtype of the lesion (ie, anaplastic). While there are these classic appearances of these lesions, in practice there is considerable overlap. Advanced magnetic resonance techniques might be useful to improve preoperative accuracy in instances where conventional imaging is not definitive (see advanced imaging section). Outcomes have improved over the last couple of years. The highly aggressive cerebellar grade 4 medulloblastoma now has a 5-year survival rate exceeding 80%. This can be attributed to refined surgical techniques and our improved ability to assess initial and residual disease with clinical imaging—both together resulting in a higher incidence of complete tumor resection and early detection and aggressive treatment of recurrent disease. The main goal of current clinical trials is to improve outcomes and quality of life for the young high-risk group of patients, where tumors tend to be more malignant and disease dissemination is more frequent, using chemotherapy regimens and by avoiding or minimizing the use of devastating radiation therapy.[4-8]

Pineal Region Lesions

There is a large differential lesions in the pineal region, and germ cell tumor is the most common type. They are hypercellular tumors that are hyperdense on noncontrast CT, may be calcified on CT, and are hypointense on T2 imaging (Figure 3). Germ cell tumors may be pure germinoma or mixed-type lesions. Different malignant germ cell tumors include embryonal carcinoma, endodermal sinus tumor (yolk sac tumor), and choriocarcinoma. Other more benign germ cell tumors include immature and mature teratomas. Pinealblastoma can be seen in patients with retinoblastoma. Other types of lesions in the pineal region include astrocytomas and gangliogliomas. Epidermoids can also form pineal cystic lesions (Table 6; Figure 4).

Intraventricular Lesions

Pediatric intraventricular tumors may be specifically found in certain locations of the ventricles. For example, choroid plexus papillomas and choroid plexus carcinomas may be found in the atrium of the lateral ventricles. The difference between papillomas and carcinomas can be usually distinguished by conventional MRI criteria including (1) the size of the lesion, (2) the degree of surrounding vasogenic edema, and (3) the invasiveness of the lesion with the margin of the ventricles (Figure 5). In some cases where the lesion cannot be clearly distinguished, magnetic resonance spectroscopy may be useful in distinguishing papillomas from carcinomas (see the advanced imaging sections). In the region of the foramen of Monro, subependymal giant cell astrocytomas may be found typically associated with tuberous sclerosis complex. Lesions that involved the third ventricle sometimes include lesions that arise from the suprasellar region (see below). Lesions that involve the fourth ventricle include those discussed in the posterior fossa section above.

Suprasellar Lesions

The major differential for the suprasellar region in the pediatric patient is (1) optic pathway/hypothalamic glioma, (2) craniopharyngioma, and (3) germ cell tumors. While these lesions can have distinct appearances, they can present as both mixed cystic and solid lesions. Craniopharygioma can be distinguished from the optic pathway gliomas and germ cell tumors by their predominating cystic characteristic (Figure 6). Another differentiating factor for craniopharyngiomas is that the cystic lesion can have rim calcification that can be well visualized on CT or gradient echo imaging. The calcification pattern can sometimes be heterogeneous. Germ cell tumors can be differentiated from optic pathway/hypothalamic gliomas by the characteristics of the solid portions of the lesion (Figure 7). For germ cell tumors, the solid portion of the lesion tends to be hypointense on T2 imaging

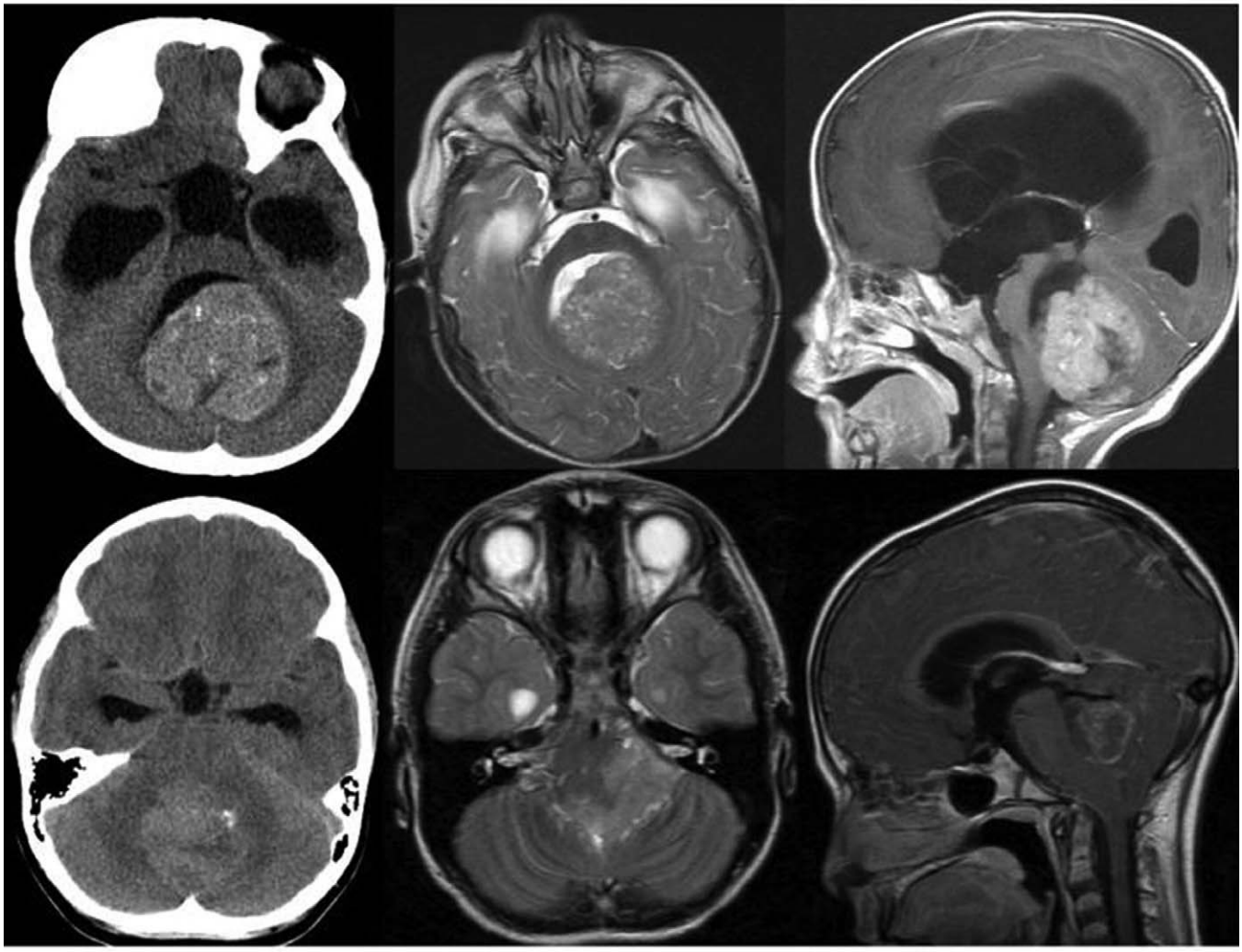

Figure 1. Comparison of medulloblastoma (premative neuroectodermal tumor; top) and ependymoma (bottom). Noncontrast CT images (left); axial T2 (middle) and sagittal postcontrast T1(right). Premative neuroectodermal tumor arising from the roof of the fourth ventricle and demonstrates hyperdensity on noncontrast CT and low signal on T2 imaging, which is indicative of hypercellular tumor. In contrast, ependymoma arise from the floor of the fourth ventricle and tend to extend into the foramen Lusaka or Magendie. The density and signal characteristic of ependymoma are variable with respect to cellularity.

(hypercellularity) compared to hyperintense on T2 imaging for optic pathway/hypothalamic tumors (which tend to be pilocytic astrocytomas that are hypocellular; Figure 2). When the lesion is confined to the infundibulum, the differential for this lesion is usually that of Langerhans cell histocytosis, germ cell tumors, lymphocystic hypophysitis, and other inflammatory conditions.

Supratentorial Lesions

Tumors which present in the posterior fossa can also present in the supratentorial regions. This includes primitive neuroectodermal tumor, pilocytic astrocytoma, and ependymoma. Atypical teratoid rhabdoid tumors may be found either supratentorially or infratentorially. Of note, occasionally, atypical teratoid rhabdoid tumors may be associated with rhabdoid tumors of the kidney (Figure 8). Some astrocytoma subtypes may present in both the supratentorial and the infratentorial including fibrillary (diffuse) astrocytomas, low-grade astrocytomas, anaplastic astrocytomas, and glioblastoma multiformis. Other astrocytic subtypes tend to present only supratentorially including pleomorphic astrocytomas and subependymal giant cell astrocytomas. Ganglion cell tumors including gangliogliomas and dysembryoplastic neuroepithelial tumors are usually found supratentorially (Figure 9). Germ cell tumors that normally present in the pineal and suprasellar regions may also present in the basal ganglia and are sometimes associated with hemiatrophic changes to the ipsilateral cerebral hemisphere.

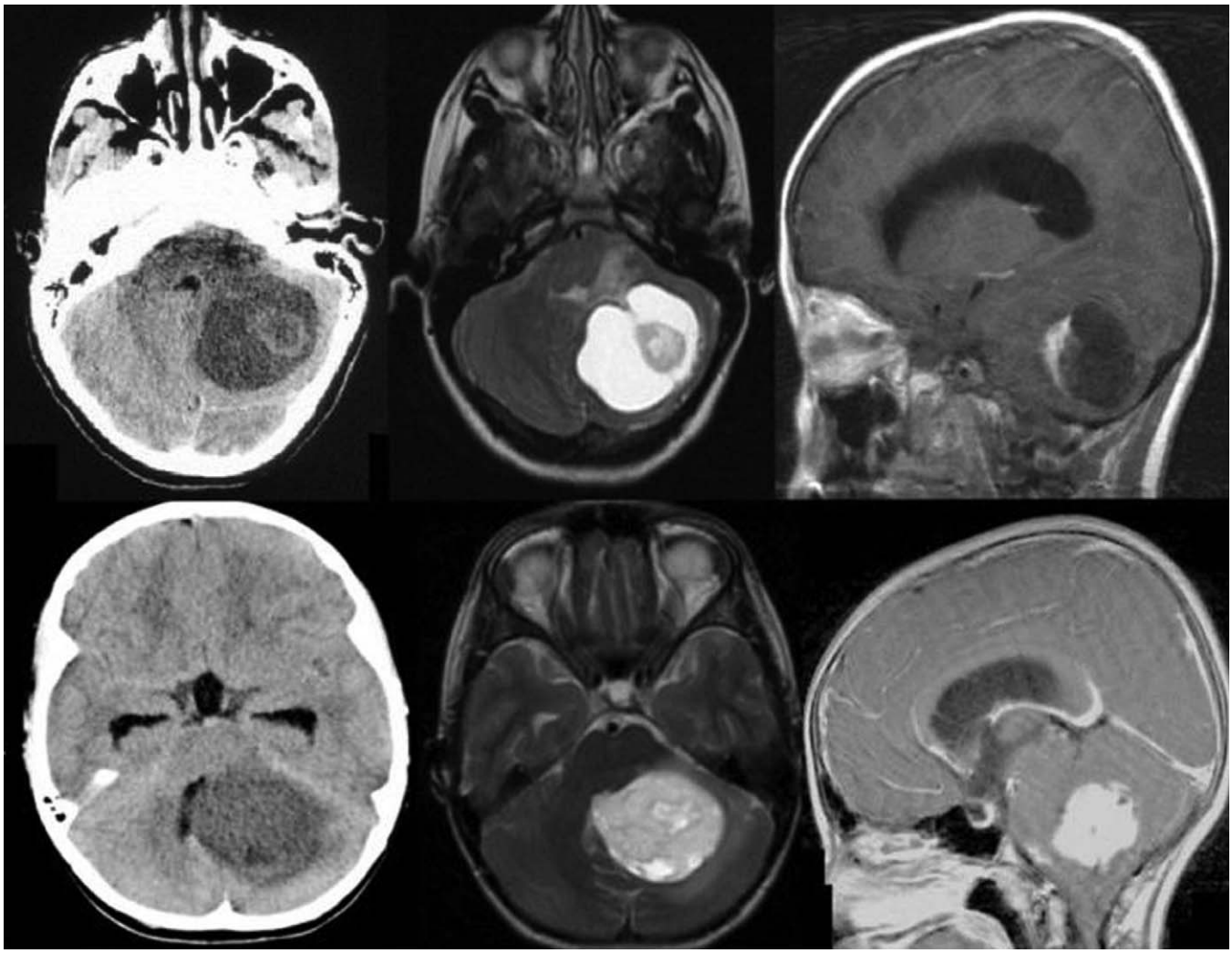

Figure 2. Variation in the appearance of pilocytic astrocytomas. A more cystic juvenile pilocytic astrocytoma (top) compared to a more solid juvenile pilocytic astrocytoma (bottom). Noncontrast CT images (left); axial T2 (middle) and sagittal postcontrast T1 (right). A common feature of pilocytic tumors in that the solid portions of the tumor tend to demonstrate hypodensity on CT imaging and high T2 signal, which is indicative of hypocellularity (in contrast to premative neuroectodermal tumor from Figure 4).

Cerebellar Pontine Angle Lesions

The most typical well-known cerebellar pontine angle lesion in the bilateral schwannoma is typically seen in patients with neurofibromatosis 2. However, in the pediatric case, there are other lesions which can present in the internal auditory canal region, including metastatic lesions (rhabdomyosarcoma and neuroblastoma), primary neuroepithelial tumors, or hemangiomas.

Brain Stem

The lesions that present in the pediatric brain stem (Table 7) vary significantly in appearance and prognosis depending on the location of the brain stem. The most common brain stem lesion is that of the diffuse intrinsic brain stem gliomas (also termed diffuse pontine gliomas; Figure 10). These tumors which are centered in the pons can often be low-grade lesions at presentation, are inoperable because of their location, and are highly resistant to radiation or chemotherapies.[9-14] They have the worst prognosis of all tumors in pediatric neuro-oncology. Mortality is practically 100%, and more than 50% of the patients die within 12 months after initial diagnosis. There has been no improvement in survival for several decades for these tumors. Other lesions in the brain stem tend to have a better prognosis and are thought predominately to be low-grade astrocytomas or pilocytic astrocytomas. The tectum is a common place for astroctyomas (Figure 10). The lesions in the cervical medullary region and medullopontine region tend to have a dorsally exophytic growth pattern and tend to be pilocytic astrocytomas.

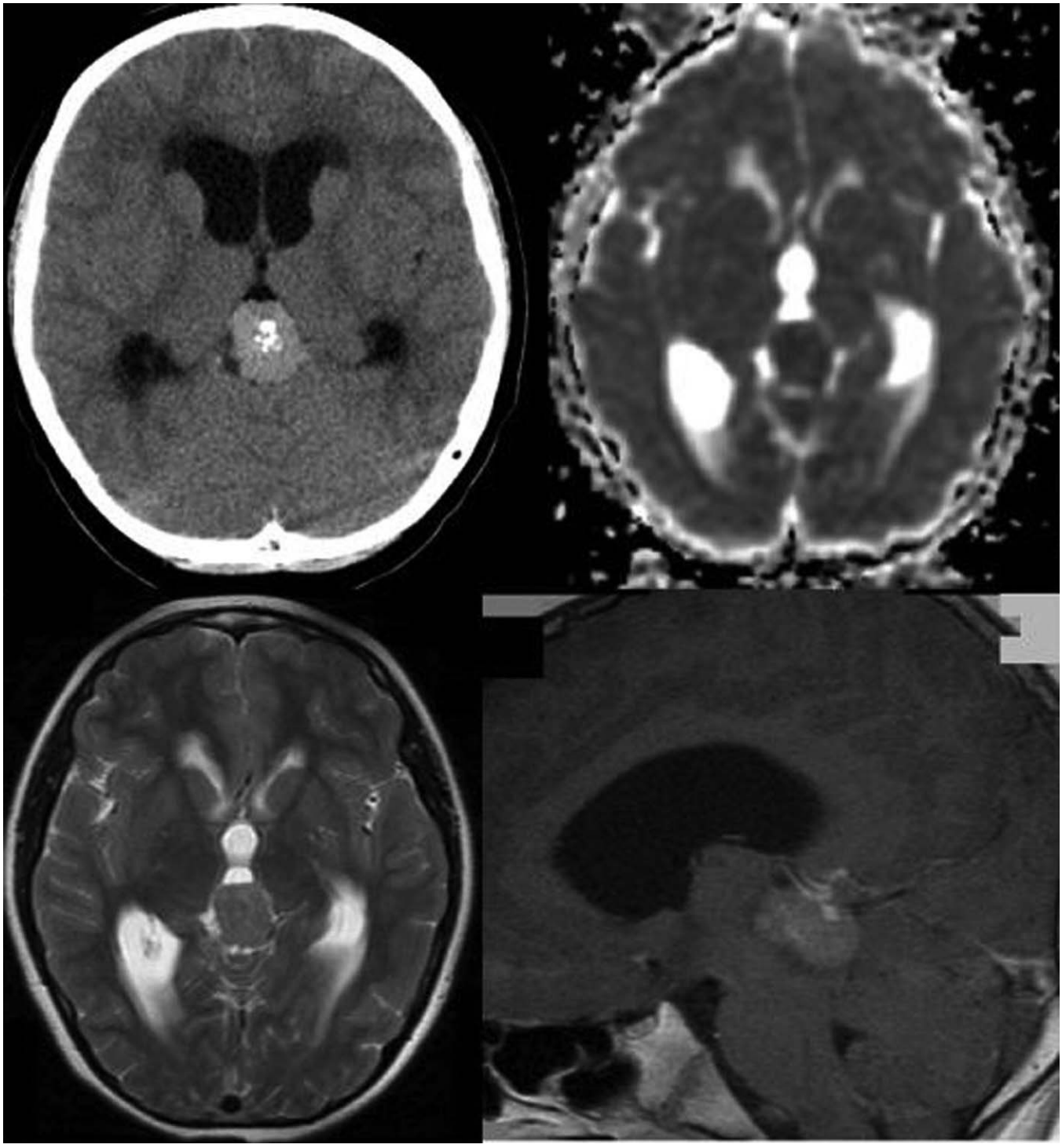

Figure 3. Pineal germinoma. Noncontrast CT (top left); apparent diffusion coefficient diffusion map (top right); axial T2 (bottom left) and postcontrast sagittal T1 (bottom right). The lesion's calcification is best seen on computed tomography (CT) imaging. In addition, the solid portion of the lesion is hyperdense on noncontrast CT, demonstrating low apparent diffusion coefficient signal, and low T2 signal which are all indicative of a hypercellular tumor (compare to premative neuroectodermal tumor from Figure 4).

Table 6. Common Pineal Region Lesions

Germ cell tumors
Germinoma
Teratoma
Mixed germ cell tumors
Pineal parenchymal cell tumors
Pineocytoma
Pineoblastoma
Other cell tumors and neoplastic-like masses
Pineal cysts
Astrocytoma
Vein of Galen fistula
Other (lipoma, epidermoid, arachnoid cyst)

Noncontrast CT Imaging for Detection of Tumors

Hyperdense lesions on CT, which are not necessarily calcified, correspond to hypercellular tumors including premative neuroectodermal tumor, germ cell tumor, choroid plexus carcinoma, and anaplastic astrocytoma. Hyperdensity on noncontrast CT corresponds to low T2 signal, bright diffusion signal (diffusion restriction), and low apparent diffusion coefficient signal.

Introduction to Advanced Magnetic Resonance Techniques

Diffusion-Weighted and Diffusion Tensor Imaging

Diffusion-weighted MRI is based on the microscopic movement of water molecules in the brain tissue. Diffusion-weighted MRI is generally performed using a single shot spin-echo echo-planar imaging pulse sequences using additional diffusion gradients. These gradients result in an attenuation of signal obtained from moving water molecules. The strength of the diffusion gradient is expressed as a "b" value in units of seconds per square millimeters. In pediatric imaging, we tend to use a b value of 1000 s/mm^2. There are 2 basic imaging sequences that are being used to obtain quantitative information about water diffusion. The first method uses 2 images for each slice. The first image (b-zero image) is acquired without diffusion weighting whereas the second image (diffusion image) is acquired with identical parameters but in addition also using the so-called diffusion gradients prior to reading out the water signal. The diffusion gradients do not emphasize any spatial direction. On these second images areas with high water diffusion show low signal intensity whereas areas with low water diffusion have higher intensity. The 2 images can be combined to calculate the "Apparent Diffusion Coefficient" map. The apparent diffusion coefficient map is an instrument and magnetic resonance sequence-independent parameter. Diffusion imaging can help in the evaluation of brain lesions, with diffusion restriction seen within abscess collection and also in tumors that are hypocellular in nature (ie, premative neuroectodermal tumor; Figure 11).

The second method is termed diffusion tensor imaging.[15-22] Again a b-zero image is acquired. However, additional images (at least 6 per slice) are acquired, where each image emphasizes a different spatial direction for water diffusion. From the b-zero image and the set of diffusion-weighted images a more complete picture of the water diffusion can be obtained. Particularly, for each region, a diffusion matrix or tensor that contains information about the diffusion of water along the 6 independent directions (xx, yy, zz, xy, xz, and yz) can be computed. From this tensor, the fraction of isotropic or anisotropic can be derived. Diagonalization of the matrix provides the eigenvectors and eigenvalues of diffusion. The mean diffusivity is the average of the 3 eigenvalues, which are the measurements of the magnitude of the diffusion along the 3 principal orthogonal directions. The variance of the 3 eigenvalues is known as diffusion anisotropy. This diffusion anisotropy can be expressed using different metrics including fractional anisotropy, relative anisotropy, and volume ratio. Diffusion tensor imaging can also be used to map white matter tracts because water movement across fibers is hindered relative to water diffusion along the fibers.[23-25] By marking specific starting regions, diffusion tensor imaging can be used to generate tractography data to visualize tracts as they connect different parts of the brain.

Proton Magnetic Resonance Spectroscopy

The signal used by MRI to create anatomical maps is generated primarily by the hydrogen nuclei, also known as protons (^{1}H), of water molecules (H_2O). In contrast, ^{1}H magnetic resonance spectroscopy analyzes signal of protons attached to other molecules. Whereas for MRI only a single peak (water) is being mapped, the output of magnetic resonance spectroscopy is a collection of peaks at different radiofrequencies representing proton nuclei in different chemical environments, proportional to the number of contributing protons. The most prominent peak of the ^{1}H spectrum is *N*-acetylaspartate (NAA), which is the resonance at 2.0 ppm from 3 equivalent protons of the acetyl group of the *N*-acetylaspartate molecule. The role of *N*-acetylaspartate, and its regulation in vivo, is not well understood. In the normal brain, *N*-acetylaspartate is synthesized in neurons, diffuses along axons, and is broken down in oligodendrocytes. *N*-acetylaspartate is not only found in neurons but can also be found in low concentrations in oligodendrocyte type-2 astrocyte progenitor cells and immature oligodendrocytes. Proton

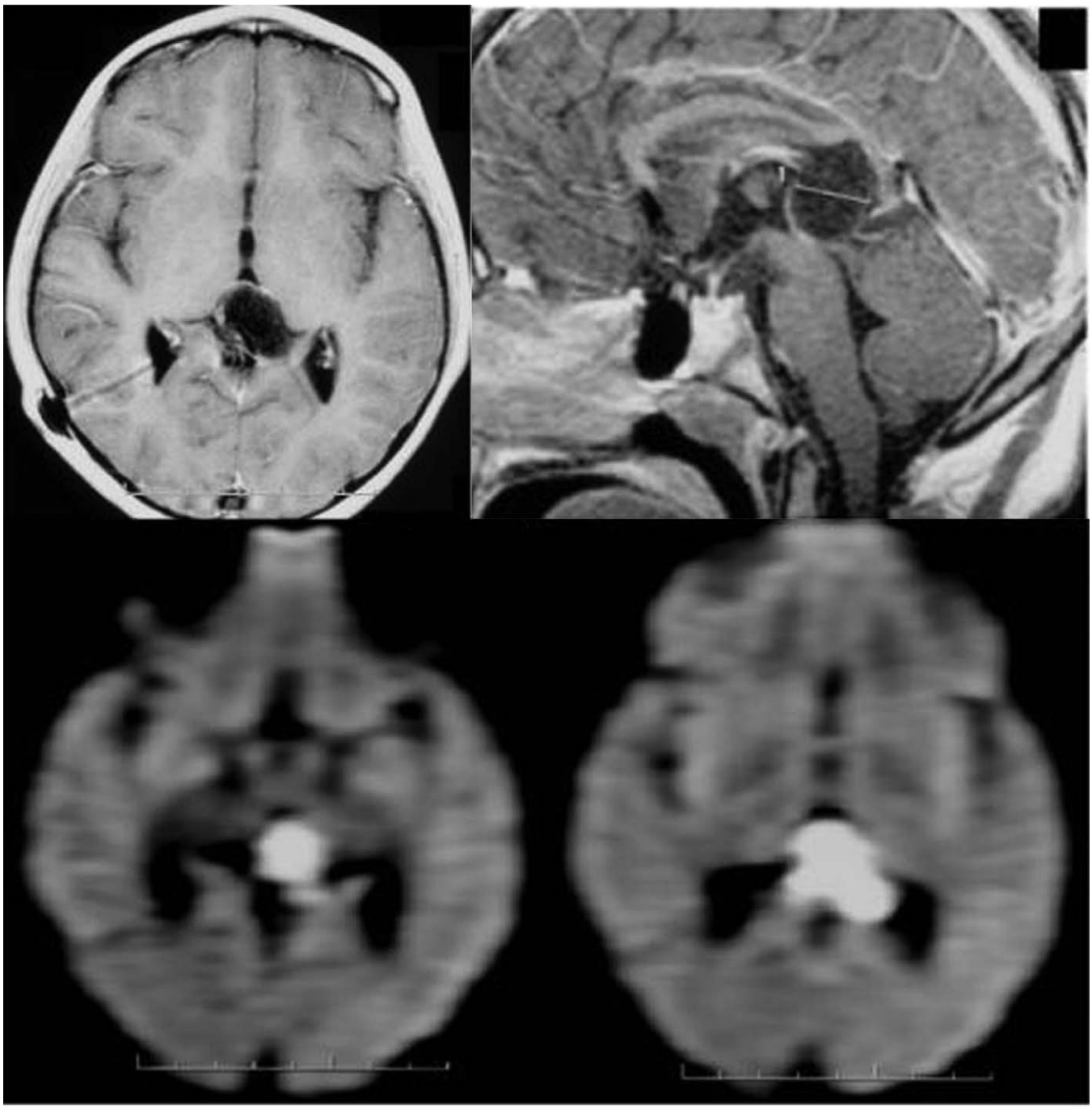

Figure 4. Pineal epidermoid. Postcontrast axial and sagittal T1 imaging showing a rim-enhancing cerebrospinal fluid signal intensity lesion in the pineal region, which could represent an arachnoid cyst (top). Axial diffusion imaging at 2 levels shows marked diffusion restriction of this cystic lesion, which is consistent with an epidermoid (bottom).

spectra of any disease that is associated with neuronal or axonal loss will exhibit a reduction in *N*-acetylaspartate.

The next prominent peak at 3.2 ppm is commonly referred to as choline or trimethylamines. Choline is a complex peak comprising several choline-containing metabolites and therefore the term *total choline* is also frequently used. Abnormal choline metabolism is a common end point for many forms of cancer. Choline-containing metabolites are involved in the synthesis and breakdown of cell membranes. Because growing tumors require the net synthesis of cell membranes to support cell proliferation, the in vivo measurement of choline provides

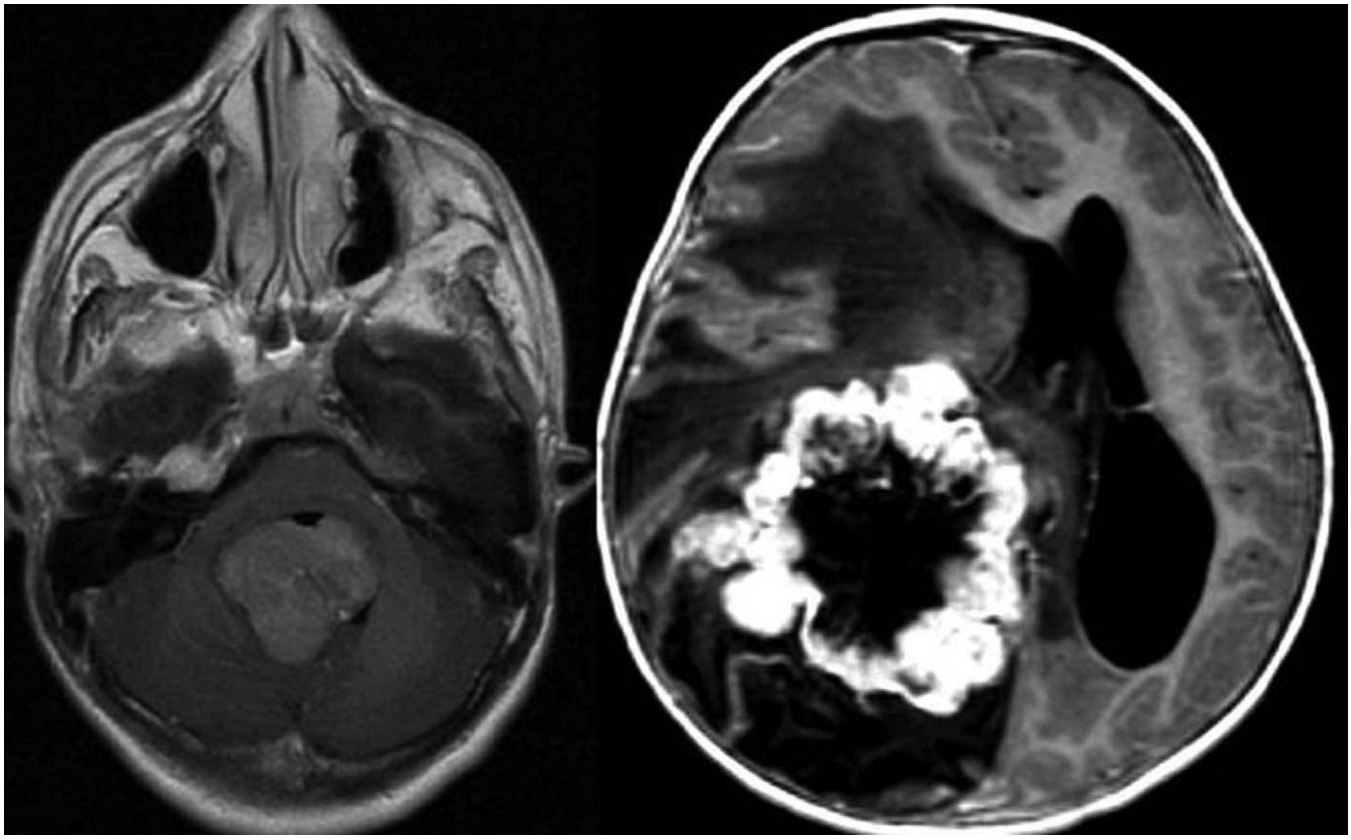

Figure 5. Choroid plexus papilloma (left) vs carcinoma (right). The major difference between the 2 lesions is the size and the invasion of the surrounding brain parenchyma, including the significant amount of vasogenic edema around the choroid plexus carcinoma lesion.

surrogate information on tumor growth rates. Brain tumors generally have elevated levels of choline. Higher choline levels have been associated with more aggressive tumors. The creatine peak at 3.0 ppm comprises both free creatine and its redox partner phosphocreatine (PCr). Phosphocreatine and free creatine are used in the tissues as a battery to replenish adenosine triphosphate (ATP) levels in situations where high energy demand is not met by cellular energy production. Total choline, creatine, and *N*-acetylaspartate can be detected readily and quantified in long *echo time* magnetic resonance spectroscopy. Short echo time acquisition methods are necessary for reliable quantitation of *myo-inositol*. Myo-inositol is a little-known sugar-like molecule that resonates at 3.6 ppm in the proton spectrum. It has been identified as a marker for astrocytes and is an osmolyte.[26,27] Myo-inositol is also involved in the metabolism of phosphatidyl inositol, a membrane phospholipid. Similar to choline, myo-inositol is expected to be altered in response to alteration of membrane metabolism or damaged membrane.

Lactate is an important metabolite because it indicates anaerobic metabolism. Although lactate can be detected at pathologically elevated concentrations, in healthy tissue the lactate concentration is too low for routine detection with currently available methods. An important exception is newborns (particularly premature newborns) where lactate is detectable in apparently normal brain tissue.[28] It is enough that pyruvate dehydrogenase the enzyme that enables the entry of pyruvate into the tricarboxylic acid cycle has a low activity in early brain development. Lactate is the product of anaerobic glycolysis and increases when subsequent oxidation of lactate in the tricarboxylic acid cycle is impaired (for example by lack of oxygen or mitochondrial disorders). Lactate can also increase in necrotic tissue and cysts.

The protons of the methyl groups ($-CH_3$) of lipid molecules resonate at 0.9 parts per million (ppm) whereas protons of the methylene groups ($-CH_2-$) resonate at 1.3 ppm in the ^1H spectrum. Both the resonances are broad and may also comprise contributions from other macromolecules. In normal tissue, the concentration of free lipids is small and there should be very little signal in this part of the spectrum. Lipid signals increase when there is breakdown of cell membrane and release of fatty acids. Lipids are therefore important markers for severe brain injury.

Magnetic resonance spectroscopy can be performed using either single-voxel or multivoxel techniques (also

Figure 6. Variation in the appearance of craniopharyngioma. Classic rim-calcification pattern associated with a suprasellar predominately cystic mass (top). More solid heterogenous calcified mass with more solid components (bottom).

referred to as chemical shift imaging). At Childrens Hospital Los Angeles single-voxel magnetic resonance spectroscopy acquisition mode was selected in most studies over chemical shift imaging, where many spectra covering a larger volume of the lesion are acquired simultaneously. This ensures that the quality of individual tumor spectra would not be affected adversely by unavoidable compromises accompanying chemical shift imaging acquisitions from larger volumes. In particular for infratentorial tumors, good magnet field homogeneity and water suppression is not always achieved uniformly. In addition, chemical shift imaging requires the processing and review of many spectra and offers voxel shifting. While in principle this should be considered to be an

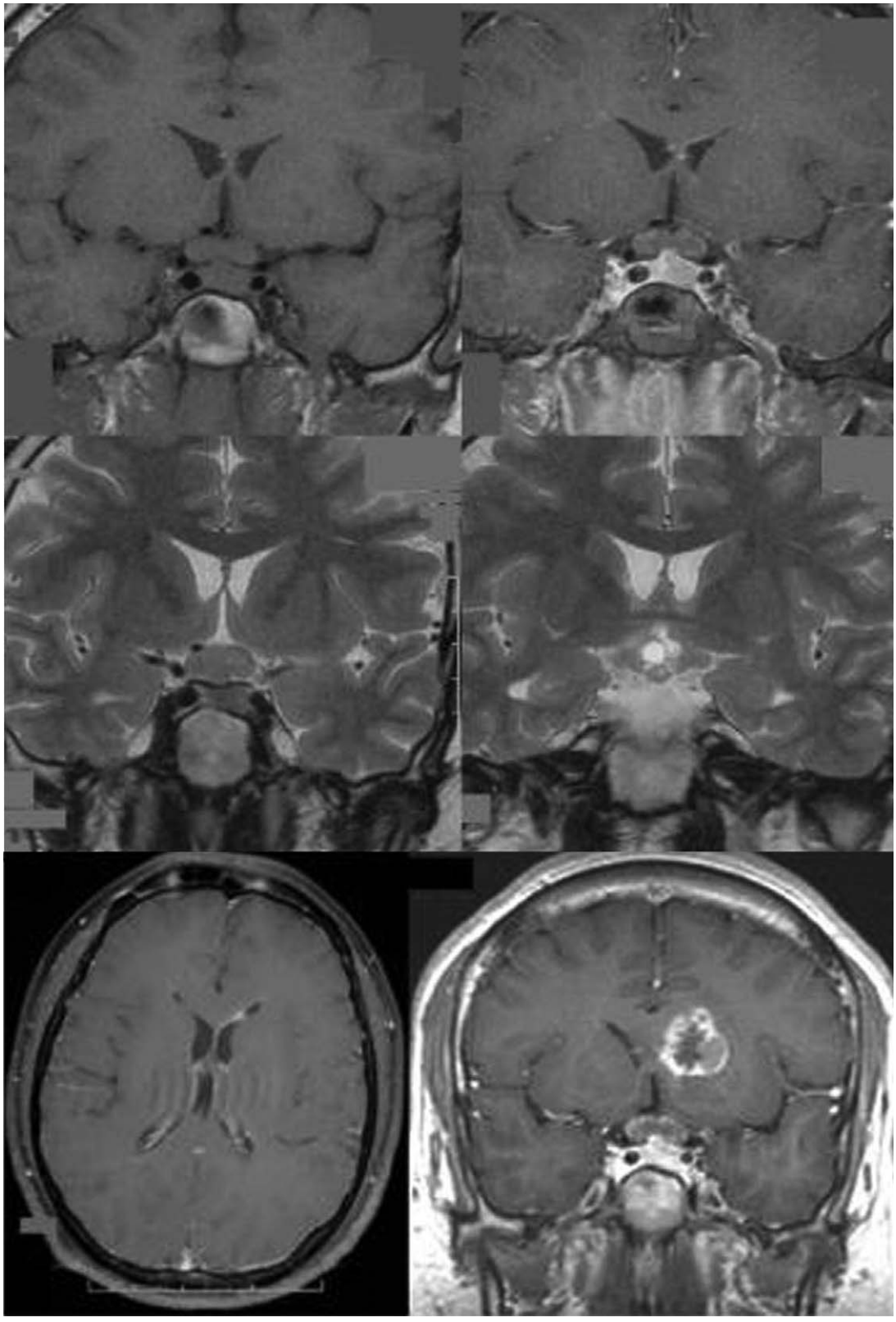

Figure 7. Suprasellar germinoma. Images show an enhancing suprasellar mass that appears to be chiasmatic and originally diagnosed as an optic pathway glioma (top). T2 images show that the lesion has low T2 signal within it and multiple small cyst more posteriorly, which is more consistent with a hypercellular tumor like a germ cell tumor (middle). Postcontrast axial T1 imaging of an initial scan also shows a small focus of left frontal horn subependymal seeding, which is more consistent with a germ cell tumor (with growth on the follow-up scan; bottom).

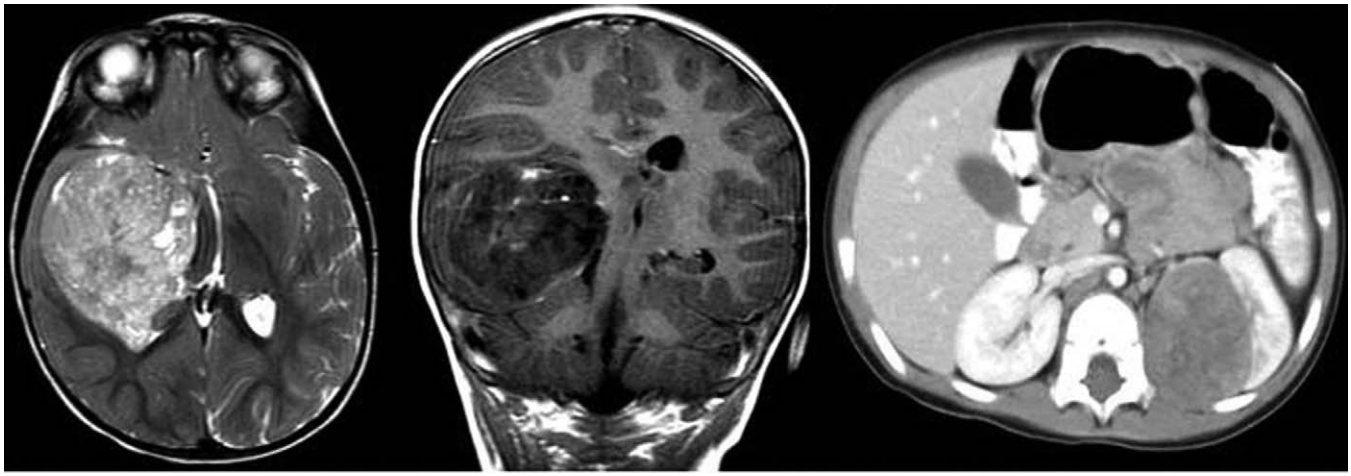

Figure 8. Supratentorial atypical teratoid rhabdoid tumor with rhabdoid tumor of the kidney. Axial T2 (left), coronal postcontrast T1 (middle); axial computed tomography (CT) of the abdomen at the level of the kidneys (right).

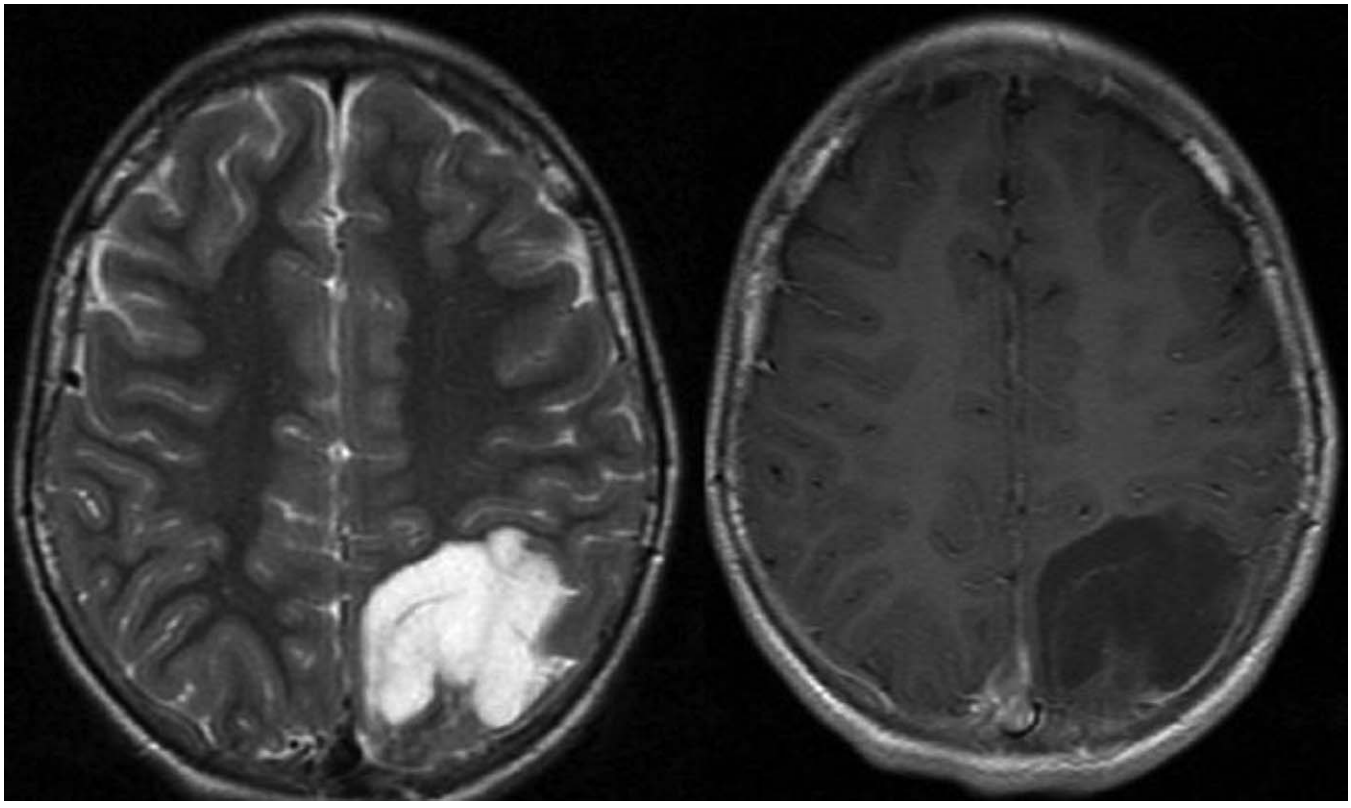

Figure 9. Dysembryoplastic neuroepithelial tumors. This lesion is usually cortically based, well circumscribed, minimally enhancing with very high T2 signal. Sometimes the lesion is associated with scalloping of the inner table of the calcarium.

advantage over single-voxel magnetic resonance spectroscopy, in practice, processing and quality control of chemical shift imaging is more time-consuming and requires the expertise of a skilled magnetic resonance spectroscopist. Thus, chemical shift imaging is often not feasible in environments where resources are sparse.

Perfusion Magnetic Resonance

There are 2 major classes of magnetic resonance techniques that can measure perfusion in the brain. The first class, dynamic susceptibility enhanced perfusion MRI, is based on the use of intravascular contrast agents that can

Table 7. Pediatric Brain Stem Gliomas[a]

Tumor Type	Approximate Frequency (%)	Imaging Characteristics	Predominant Pathology
Diffuse intrinsic	75-85	Diffuse pontine enlargement, T1 hypointensity, T2 hyperintensity, little contrast enhancement	Fibrillary astrocytoma (grades 2-4)
Focal midbrain	5-10	Small, well-circumscribed, no edema, T1 hypointensity, T2 hyperintensity, bright enhancement	Low-grade astrocytoma (grade 1 and 2), ganglioglioma
Dorsally exophytic	10-20	Arise from floor of 4th ventricle, T1 hypointensity, T2 hyperintensity, bright enhancement	Pilocytic astrocytoma (grade 1), grade 2 astrocytoma
Cervicomedullary	5-10	Arise from lower, medulla/upper cervical cord, bulges dorsally toward 4th ventricle, T1 hypointensity, T2 hyperintensity, commonly enhances	Low-grade astrocytoma, ganglioglioma

a. Adapted from Pan and Prados (2004)[12] [Adapted from Freeman and Farmer (1998)[10]].

change the magnetic susceptibility of blood causing a change in magnetic resonance signal. Commonly used are paramagnetic substances such as gadolinium, which do not cross the normally intact blood–brain barrier. In a typical acquisition, rapid gradient echo or spin-echo echo-planar technique methods (≈1 image every 100 ms) are used to obtain susceptibility (T2*)-weighted MRIs. After approximately 20 seconds into the scan, the contrast agent is injected intravenously into the blood stream with a power injector or by hand. The contrast agent containing the blood passes through the tissue and causes a signal drop that is, in first order, proportional to the blood volume. The signal change during the first transit of the contrast through the tissue is measured relative to the set of precontrast baseline scans. This signal intensity/time activity curve is then used to calculate the relative cerebral blood volume, relative cerebral blood flow, and mean transit time.

The second, arterial spin labeling arterial blood is tagged by a single or a series of radiofrequency pulses. These pulses essentially render arterial blood dark and result in a signal attenuation proportional to the blood flowing into the tissue on MRIs.[29-37] An important feature of arterial spin labeling is that it allows the quantitation of cerebral perfusion without the use of exogenous contrast agents. However, signal intensity changes are comparably small (when compared with methods using contrast agents) and depend on additional parameters such as the T1 relaxation time of blood and the time delay between the tagging pulses and the readout time of the images. The 2 major types of arterial spin labeling are pulsed arterial spin labeling and continuous arterial spin labeling.[32-36] The pulsed arterial spin labeling sequence is obtained by transmitting a 180-degree radiofrequency pulse during a very short period of time to a large slab proximal to the area of interest. This pulse results in "labeling" of the water protons of the arterial blood by inverting their magnetization. Then as the blood flows into the arterioles and the capillaries, the magnetization of the water molecules results in the change of total magnetization within the tissue. As for dynamic contrast-enhanced perfusion imaging, a fast echo-planar imaging is used to image the region being perfused by the blood after a certain time delay. The same sequence is then repeated without labeling the arterial water protons and the 2 images are subtracted to generate a quantitative flow map. A quantitative perfusion map is calculated by mathematical formulas that take into account the difference in magnetization/signal intensity between the labeling image and the unlabeling images and relate it to regional cerebral blood flow. A continuous arterial spin labeling sequence uses the same type of sequences except that the blood is contiguously tagged for a longer period of time on a thinner slab of tissue that is farther away from the imaging slice compared to the pulsed arterial spin labeling technique.

Each of the methods discussed above is sensitive to specific perfusion states of tissue, with the contrast method proving the best measurement of cerebral blood volume, and the arterial spin labeling technique provides the best measurement of cerebral blood flow.

Applications of Advanced MRI in Pediatric Brain Tumors

Advanced magnetic resonance techniques may be used in (*a*) improving the accuracy of initial diagnoses; (*b*) evaluating the risk at initial diagnosis; and (*c*) monitoring the effectiveness of therapy.

Improvement of Accuracy of Initial Diagnosis

Posterior Fossa Tumors

Approximately 50% of all pediatric tumors arise from the posterior fossa. In most cases, these tumors are grade 4 medulloblastomas, grade 1 pilocytic astrocytomas, or (less frequently) grade 2 or 3 ependymomas. Although the medulloblastoma tends to have low signal intensity on T_2-weighted images, indicating a hypercellular tumor,

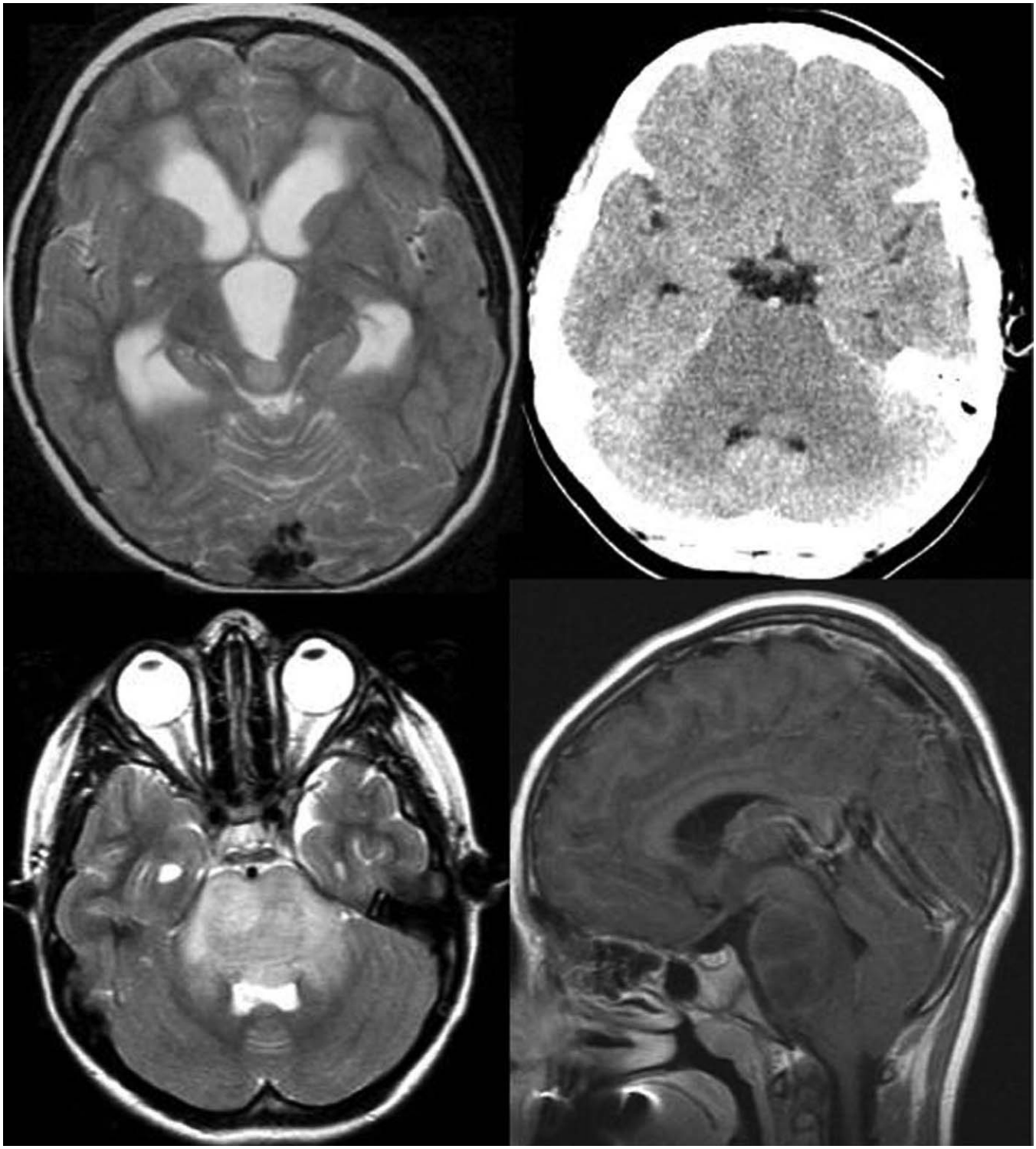

Figure 10. Tectal glioma and diffuse instrinsic pontine glioma. Axial T2 showing a tectal mass resulting in obstructive hydrocephalus (top left); noncontrast computed tomography (CT) showing expansive hypodensity in the pons consistent with a pontine glioma (top right). At presentation, these lesions demonstrate high T2 signal (bottom left) and are nonenhancing (bottom right).

there are instances in which ependymoma may present with similar features. It is common that ependymoma involve the fourth ventricular floor and extend into the foramen of Luschka. However, large medulloblastomas may have a similar growth pattern. Occasionally, a cystic/necrotic medulloblastoma may have imaging

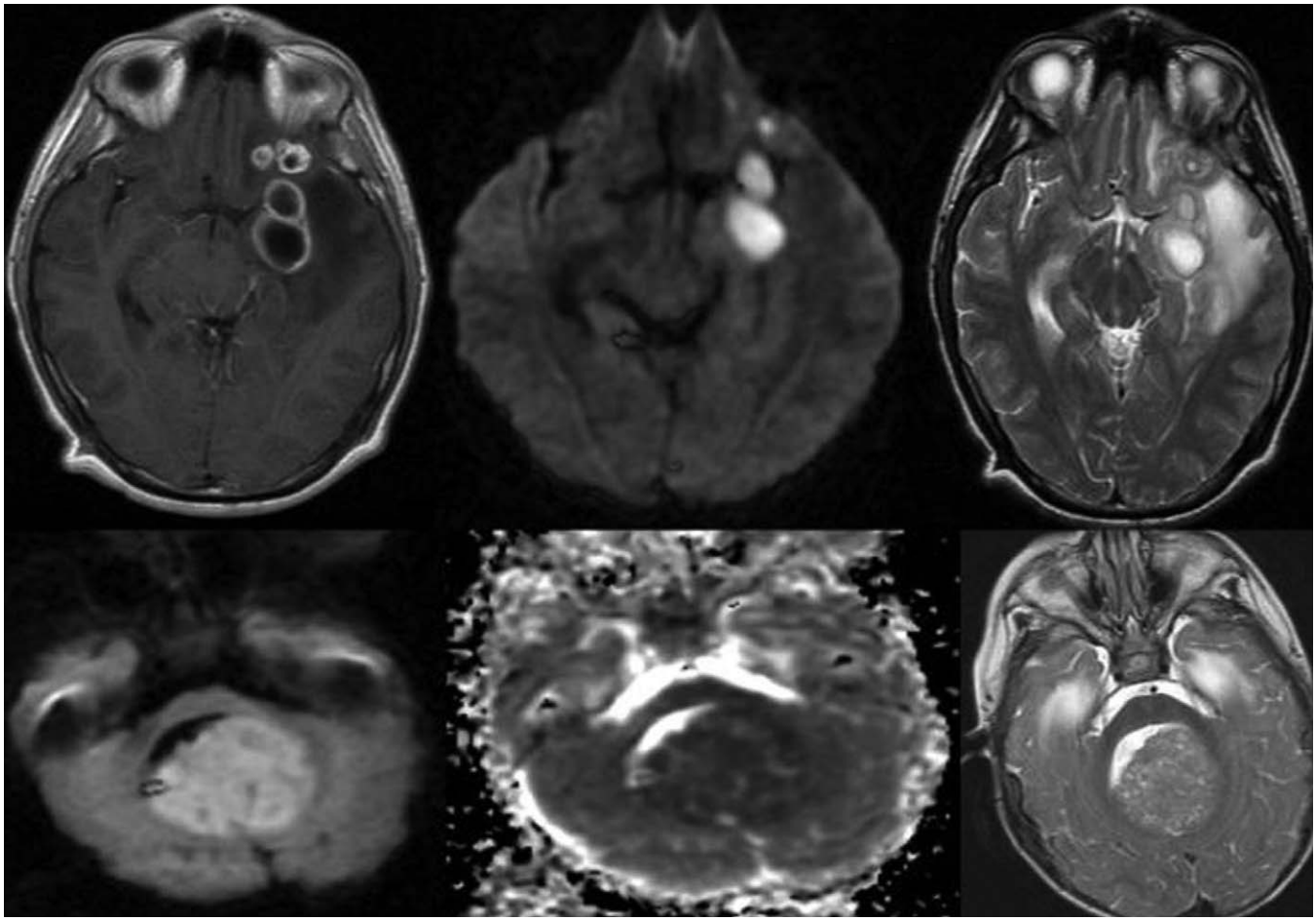

Figure 11. Diffusion imaging in detecting abscess collection (top) compared to hypercellular tumor (bottom). Rim-enhancing cystic lesion that restricts diffusion and a low T2 signal rim is pathonomonic for an abscess (top left). High diffusion signal (bottom left) with low apparent diffusion coefficient (bottom middle) and a solid mass which has low T2 signal consistent with a hyperceullar tumor (premative neuroectodermal tumor, see Figure 4).

characteristics that overlap with posterior fossa pilocytic astrocytoma. Proton spectroscopy and diffusion imaging appear to be particularly useful for diagnosis. Taurine (Tau) has been consistently observed by several groups in medulloblastoma[38-41] and is an important differentiator of medulloblastoma from other tumors of the posterior fossa. The hallmarks of pilocytic astrocytomas are very low creatine concentrations, low myo-inositol, and low total choline concentrations consistent with their low cellularity. Lipids are also low in pilocytic astrocytomas but mean lactate levels are higher than in other tumors. Ependymomas have higher myo-inositol than medulloblastomas or pilocytic astrocytomas and their choline levels are variable but fall generally between medulloblastoma and pilocytic astrocytoma. Because medulloblastoma is hypercellular whereas pilocytic astrocytoma is hypocellular, they have significantly different diffusion properties. Several published studies reported no overlap in the apparent diffusion coefficient for medulloblastoma and pilocytic astrocytoma.[42] Ependymoma is medium cellular and apparent diffusion coefficient falls between apparent diffusion coefficient values of medulloblastoma and pilocytic astrocytoma. High-grade medulloblastomas are also highly perfused tumors with high regional cerebral blood volume relative to control tissue. Despite being low-grade lesions, regional cerebral blood volume measurements in juvenile pilocytic astrocytoma indicate that the regional blood volume of this slowly growing tumor is close to or above that of normal brain tissue and can mimic high-grade lesions.[43] Very few perfusion measurements have been performed in ependymoma. Cha et al[44] reports high perfusion, however, we have been unable to confirm this in a small number of patients studied at Childrens Hospital Los Angeles and perfusion is possibly variable in this tumor type. In addition to those more common pediatric brain tumors (Table 8), occasionally other tumors may grow in the posterior fossa. The examples of posterior fossa tumors shown in Figure 12 also include a

Table 8. Advanced Magnetic Resonance Characteristics of Pediatric Brain Tumors[a]

Tumor Type	Key Metabolic Features	Appearance on MRI, Enhancement, Diffusion, and Perfusion Properties
Embryonal tumors		
Medulloblastoma	High taurine, *N*-acetylaspartate depleted, total choline generally prominent, lipids prominent inmost cases	Either solid or cystic cellular lesions with compromised blood-brain–barrier, generally enhancing, restricted diffusion (low apparent diffusion coefficient), generally well perfused (high regional cerebral blood volume)
Desmoblastic medulloblastoma	Similar to classic medulloblastoma —but taurine not always observed	
Supratentorial primitive neuroectodermal tumor	Similar to classic medulloblastoma	
Atypical teratoid rhabdoid tumor	Choline not as prominent as in classic medulloblastoma in some cases, taurine not observed, lipids highly variable	
Pilocytic astrocytoma	Generally low concentrations, creatine particularly low, no evidence for taurine, low myo-inositol, residual signal at 2ppm (consistent with *N*-acetylaspartate), high *N*-acetylaspartate/creatine, high total choline/creatine. No major metabolic differences between posterior fossa lesions and lesions elsewhere in the brain. Absence of taurine, low creatine, low total choline separates posterior fossa pilocytic astrocytoma from medulloblastoma	Often cystic lesions, bright on T2-weighted MRI due to low cellularity, enhancing after contrast administration; relative unrestricted diffusion (high apparent diffusion coefficient) and perfusion close to that of normal tissue; high apparent diffusion coefficient distinguishes between posterior fossa pilocytic astrocytoma and medulloblastoma
Astrocytoma		
Grades 2, 3 Glioblastoma	No evidence for taurine, increasing total choline and decreasing creatine/total choline with increasing grade, however significant overlap; lipids low in grade 2, 3 but often observed in grade 4 glioblastoma; myo-inositol less prominent in glioblastoma	Grades 2, 3 mostly nonenhancing, higher grade lesions have likely reduced diffusion and increased perfusion, increased likelihood for cystic/necrotic components and enhancement in glioblastoma; regional cerebral blood volume higher and apparent diffusion coefficient lower in higher grade lesions; however significant variation within tumors of same grade and even within same tumors
Diffuse intrinsic brainstem glioma	Low total choline, high myo-inositol, high citrate at presentation; choline and lipids increase over time and citrate decreases; changes consistent with malignant degeneration	Mostly non-enhancing, unrestricted diffusion (high apparent diffusion coefficient), low perfusion (low regional cerebral blood volume) at presentation, enhancement may or may not be observed at follow-up, diffusion generally decreases and perfusion increases over time
Ependymoma		
Regular (grade 2) Anaplastic (3)	High myo-inositol, no or minimum residual *N*-acetylaspartate, as in astrocytoma, lipids are variable and are more frequently observed than in astrocytoma, myo-inositol possibly higher in grade 3 vs grade 2	Generally enhancing heterogeneous lesions, solid parts isointense with normal tissue on T1- and T2-weighted MRI; mean apparent diffusion coefficient between medulloblastoma (low) and pilocytic astrocytoma (high) and regional cerebral blood volume variable
Choroid plexus tumors		
Papilloma Carcinoma	Striking myo-inositol, depleted creatine, moderate total choline levels Readily distinguishable from papilloma by high choline, and moderate myo-inositol, creatine depleted	Choroid plexus papilloma and carcinoma are avidly enhancing, distinguished by degree of surrounding vasogenic parenchymal edema; elevated regional cerebral blood volume but significant leakage of contrast agent during the bolus phase; mild-to-moderate levels of the diffusion restriction and cellularity
Germ cell tumors		
Pure Germinoma Mixed germ cell tumors	Taurine present (not as high as in medulloblastoma), high lipids, choline moderate; magnetic resonance spectroscopy of pure germinomas outside pineal area are often of low quality Low-quality spectra with broad lines	Heterogeneous, often calcified (better detectable with CT), sometimes hemorrhagic lesions; due to hypercellularity low signal on T2-weighted MRI and low apparent diffusion coefficient; pure germinomas tend to enhance more diffusely whereas enhancement of mix germ cell tumors is heterogeneous; intermediate to high relative CBV values

(*continued*)

Table 8. (continued)

Tumor Type	Key Metabolic Features	Appearance on MRI, Enhancement, Diffusion, and Perfusion Properties
Craniopharyngioma	Metabolites depleted in cystic lesions with exception of prominent lactate; total choline and myo-inositol readily detectable in solid growing lesions	Suprasellar lobulated cystic masses with multiple rim calcifications (well visualized on CT); calcification punctuate or confluent; sellar enlargement and sellar erosions may be associated; cyst wall tends to enhance on postcontrast T1-weighted MRI; small fraction of tumor may grow more solidly

Note: MRI, magnetic resonance imaging; CT, computed tomography; CBV, cerebral blood volume
a. Readers that are interested in a more complete picture of pediatric brain tumors are referred to the WHO and NIH WebPages (http://www.who.int/en/, http://www.brainlife.org/who/2007_classification.htm, http://www.nlm.nih.gov/medlineplus/childhoodbraintumors.html) and links therein and general textbooks.

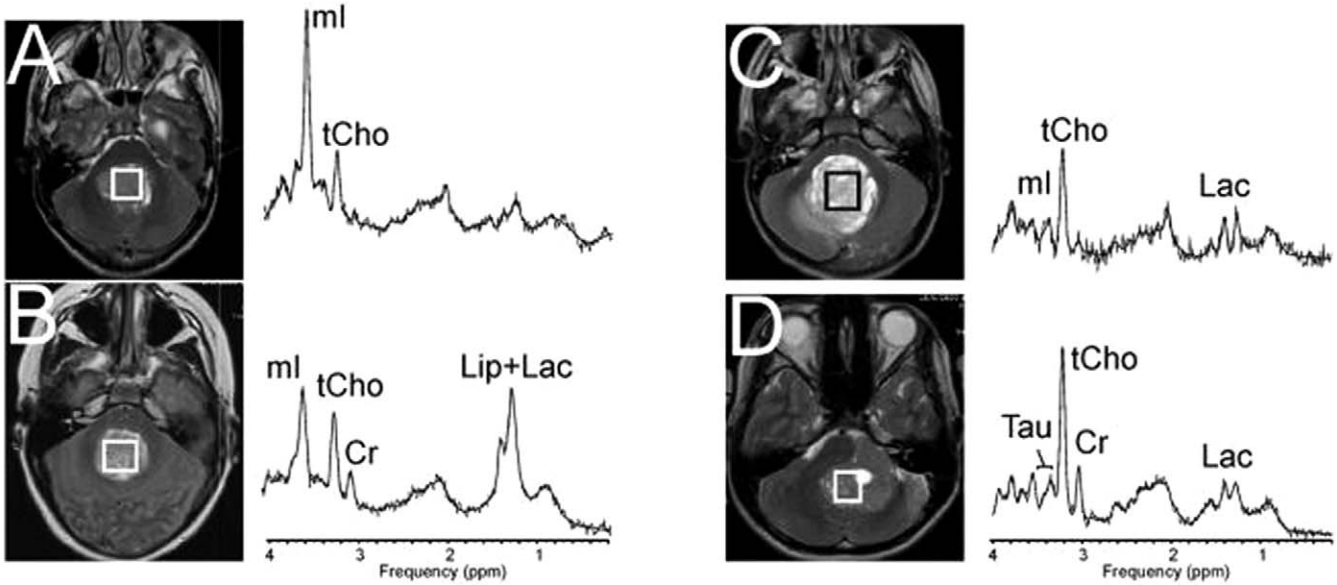

Figure 12. T2-weighted magnetic resonance images (MRIs) and magnetic resonance spectra of posterior fossa tumors. A, Choroid plexus papilloma. B, Ependymoma (grade 2). C, Pilocytic astrocytoma. D, Classic medulloblastoma. All spectra were acquired from lesions with no partial volume of surrounding tissue using a single-voxel point-resolved spectroscopy sequence with a short echo time of 35 ms. Shown are the original unfiltered spectra (thin line) and the LCModel (Stephen Provencher Inc., version 6.1-G4) fits to the data (thick line). In all 4 cases presented, the impression from conventional MRI was not confirmed by subsequent tissue analysis.

choroid plexus papilloma that has a unique metabolic profile with a strikingly prominent myo-inositol peak.

Tumors Outside the Posterior Fossa

As mentioned above, choroid plexus papilloma, do have a highly characteristic metabolic profile (striking myo-inositol) that distinguishes them readily from all other tumors but also from choroid plexus carcinoma which are cellular highly perfused tumors with very prominent choline and unremarkable myo-inositol (Figure 13).[45] Astrocytomas display a wide range of metabolic, diffusion, and perfusion characteristics even within the same grade. Mean choline concentrations increase with grade and lipids are more frequently detected in higher grade lesions but accurate diagnosis based on magnetic resonance spectroscopy alone is unreliable. For adult gliomas, there is ample evidence that regional cerebral blood volume increases and apparent diffusion coefficient decreases with increasing malignancy, and it is likely that this is also generally the case in pediatric astrocytoma. However, again, in individual patients, grade cannot be assigned based on diffusion or perfusion imaging alone. Diffuse intrinsic brain stem gliomas are not biopsied and are usually diagnosed based on clinical symptoms at presentation and MRI.[12,46-48] On physiological magnetic resonance, diffuse intrinsic brain stem gliomas are hypocellular and hypoperfused lesions with low choline and often with citrate at presentation[49,50] (Figure 14). In the vast majority of the cases,

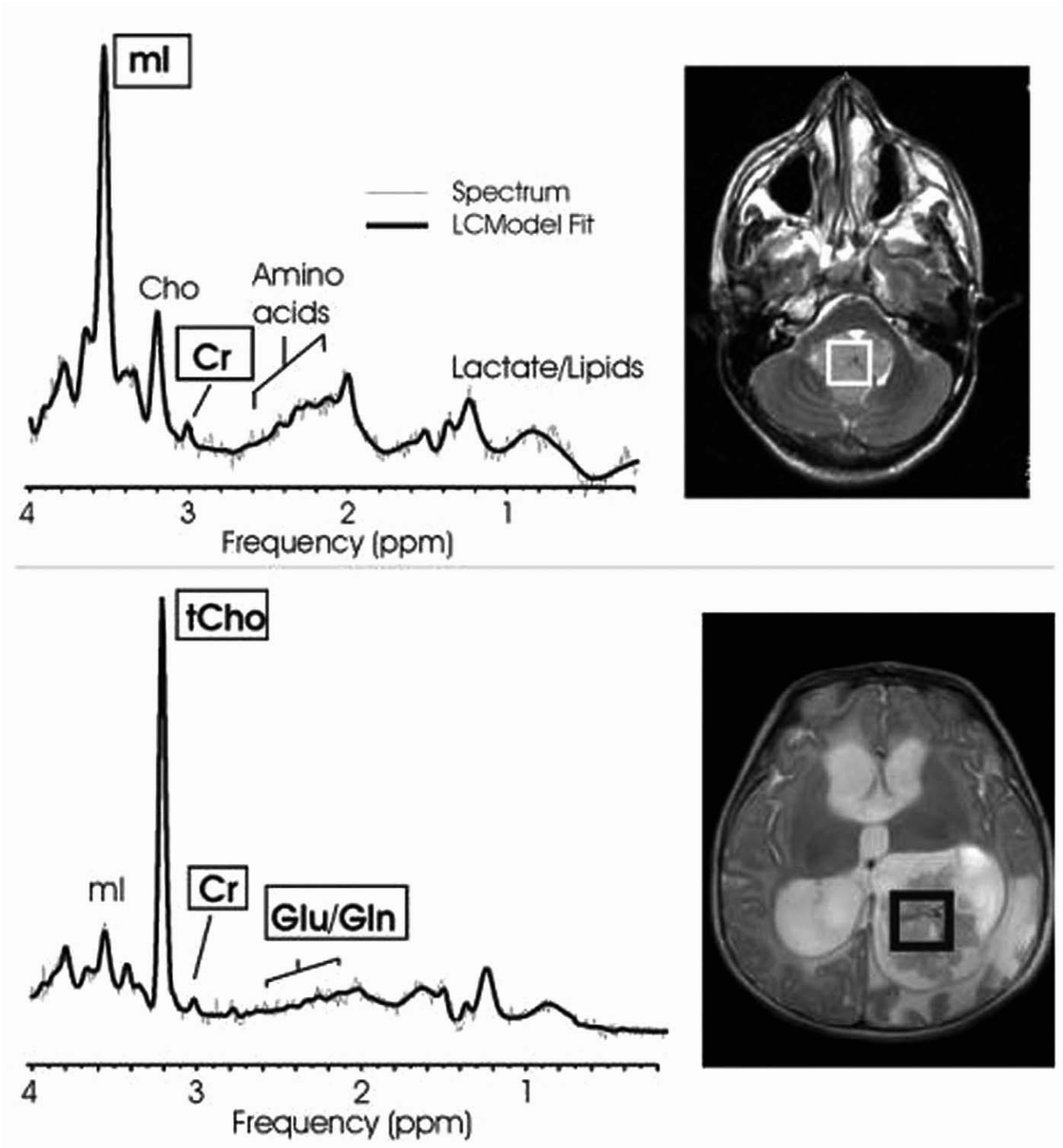

Figure 13. Choroid plexus carcinoma and papilloma can be readily distinguished by in vivo spectroscopy. Myo-inositol is elevated in choroid plexus papillomas (top left) compared to being decreased in choroid plexus carcinoma (bottom left).

conventional MRI and clinical symptoms are sufficient for diagnosis. There may be an incidence of an unusual presentation of an exophytic brain stem tumor, often a pilocytic lesion with much better prognosis, which resembles the MRI features of a diffuse tumor. In these rare occasions a magnetic resonance spectroscopy study may be necessary. Still, the significance of initial physiological magnetic resonance for these tumors is less for diagnostic purposes

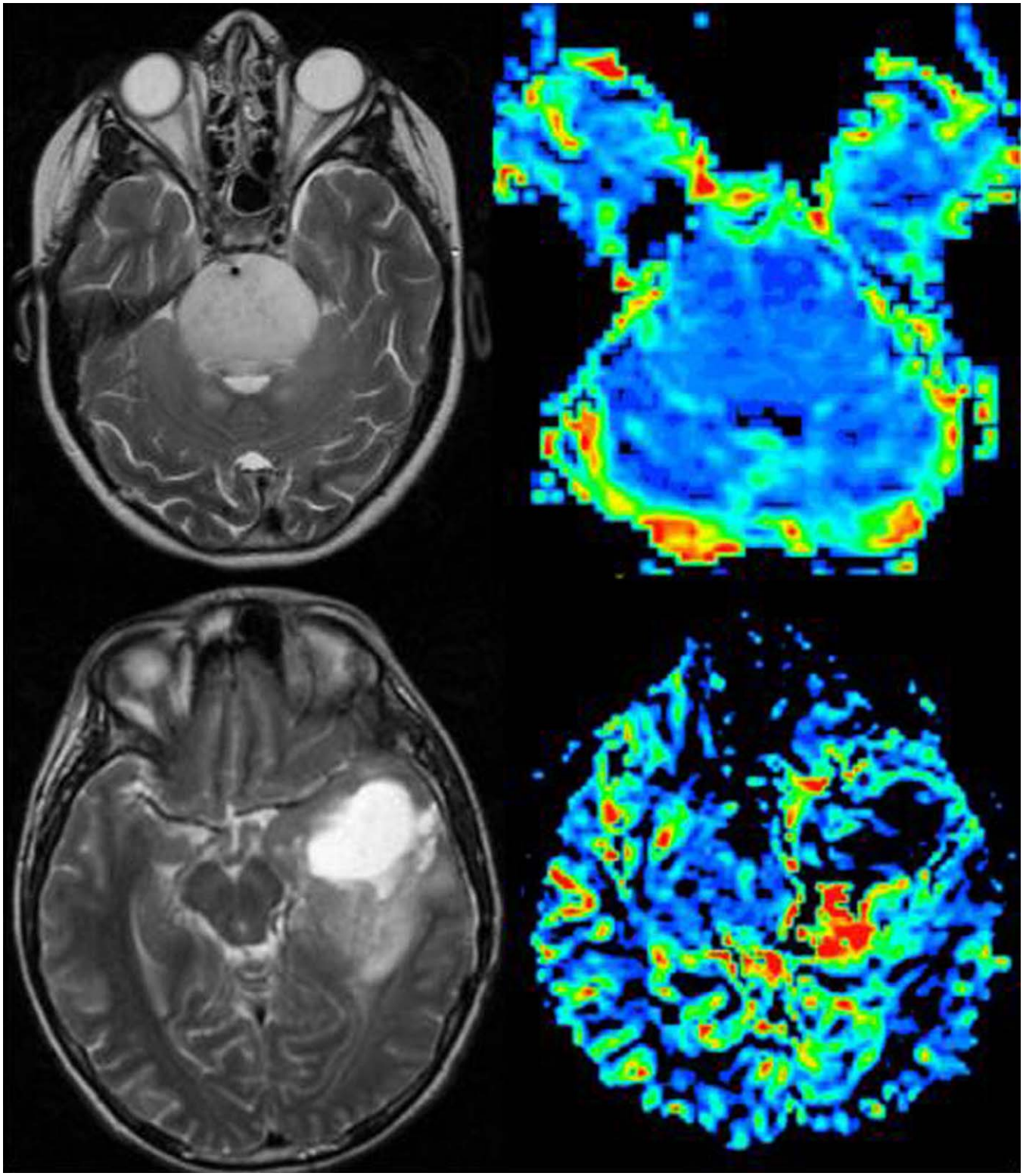

Figure 14. Perfusion magnetic resonance of pontine glioma. Dynamic contrast-enhanced imaging (gradient-echo echo-planar imaging) shows that the diffuse intrinsic pontine glioma (top) is relatively hypoperfused when compared with a left temporal supratentorial glioblastoma multiformis (bottom).

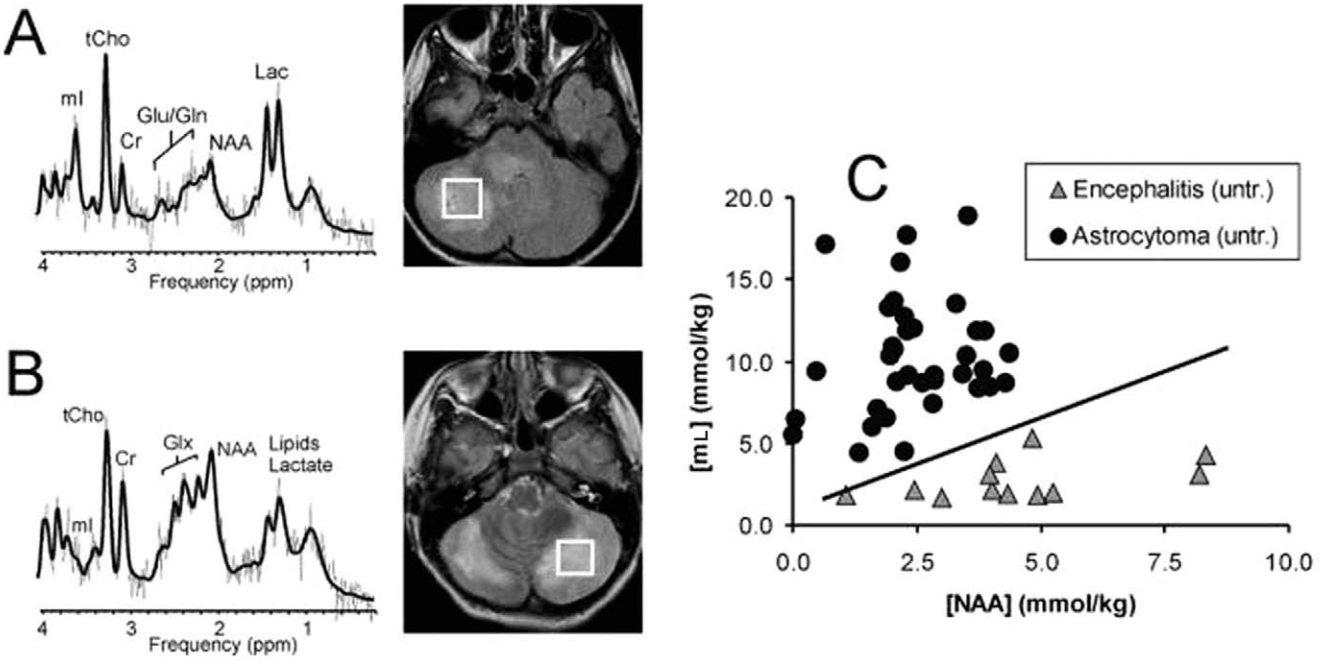

Figure 15. Single voxel-point-resolved spectroscopy (TE 35ms) spectra are consistent with multicentric glioma subsequently confirmed by biopsy and are not consistent with acute encephalitis (A). Also shown is a SV-PRESS spectrum of confirmed cerebellar encephalitis (B). Brain lesions secondary to encephalitis have a metabolic fingerprint that is significantly different from that of astrocytomas, particularly, myo-inositol is significantly lower in encephalitis than in glial tumors (C).

but more for establishing baseline characteristics that may be relevant for therapeutic monitoring.

Differentiation of Encephalitis From Astrocytomas

Accurate initial diagnoses are not only needed to distinguish different types of tumors but also to separate neoplastic from nonneoplastic disease. There are multiple other focal lesions in the brain that may mimic brain tumors on conventional anatomic MRI. Some of these lesions include infectious or inflammatory lesions, infarcts, and demyelinating lesions (tumefactive demyelinating lesion). Because of a disrupted blood–brain barrier, these lesions can demonstrate avid contrast enhancement that can mimic conventional MRI characteristics of a malignant brain tumor. Both diffusion and perfusion magnetic resonance can help distinguish these nonneoplastic lesions from neoplastic lesions. In general, these infectious and demyelinating lesions can demonstrate low-to-mild elevation of regional cerebral blood volume compared to malignant brain tumors. In the setting of an acute infarct, diffusion-weighted imaging tends to demonstrate diffusion restriction (low apparent diffusion coefficient signal) with normal or elevated T2 signal compared to hypercellular tumors that demonstrate low apparent diffusion coefficient signal associated with low T2 signal. Although there are exceptions, infectious and demyelinating lesions tend to demonstrate high apparent diffusion coefficient signal in the subacute and chronic phase. In a recent study, it was shown that brain lesions due to *acute* encephalitis have a metabolic fingerprint that is significantly different from that of astrocytoma[51] (Figure 15). Accurate noninvasive diagnosis of encephalitis is important because biopsies with the possibility of complications could be avoided.

Future Implications

Major obstacles for management and clinical research include the above-mentioned biological and physiological diversity of tumors, the small number of patients in each category due to the relatively low incidence of these tumors ($\approx$ 9 per 100 000 in the United States[52]), as well as the general difficulties of conducting clinical research in children. Current basic research focuses on identifying specific molecular targets critical for cellular changes that result in uncontrolled growth and spread—moving away from the traditional approach of administering cytotoxic agents at maximum tolerated dose. Another current strategy is to use agents that affect the environment of tumors such as antiangiogenic drugs which are likely to be effective in tumors with increased angiogenesis. However, taking advantage of the numerous new potential targets remains challenging because of the small patient populations, questions about the dosage and which targets to choose, how to get agents across the blood–brain barrier,

and how to monitor/measure response.[53] The main challenge for the magnetic resonance community is to demonstrate that physiological magnetic resonance is a pivotal tool for overcoming these bottlenecks in pediatric neuro-oncology and to contribute actively to improved patient management.

References

1. Poussaint TY. Magnetic resonance imaging of pediatric brain tumors: state of the art. *Top Magn Reson Imaging*. 2001; 12(6):411-433.
2. Poussaint TY, Rodriguez D. Advanced neuroimaging of pediatric tumors: MR diffusion, MR perfusion, and MR spectroscopy. In: Castillo M, Mukherji SK, eds. *Neuroimaging Clinics of North America*. Vol 16. No 1. Philadelphia, PA: WB Saunders; 2006:169-192.
3. Gupta N, Banerjee A, Haas-Kogan D, eds. *Pediatric CNS Tumors*. Berlin, Heidelberg, New York: Springer-Verlag; 2004.
4. Sands SA, van Gorp WG, Finlay JL. Pilot neuropsychological findings from a treatment regimen consisting of intensive chemotherapy and bone marrow rescue for young children with newly diagnosed malignant brain tumors. *Childs Nerv Syst*. 1998;14(10):587-589.
5. Dhall G, Grodman H, Ji L, et al. Outcome of children less than three years old at diagnosis with non-metastatic medulloblastoma treated with chemotherapy on the "Head Start" I and II protocols. *Pediatr Blood Cancer*. 2008;50(6):1169-1175.
6. Gardner SL, Asgharzadeh S, Green A, Horn B, McCowage G, Finlay J. Intensive induction chemotherapy followed by high dose chemotherapy with autologous hematopoietic progenitor cell rescue in young children newly diagnosed with central nervous system atypical teratoid rhabdoid tumors. *Pediatr Blood Cancer*. 2008;51(2):235-240.
7. Fangusaro J, Finlay J, Sposto R, et al. Intensive chemotherapy followed by consolidative myeloablative chemotherapy with autologous hematopoietic cell rescue (AuHCR) in young children with newly diagnosed supratentorial primitive neuroectodermal tumors (sPNETs): report of the Head Start I and II experience. *Pediatr Blood Cancer*. 2008;50(2):312-318.
8. Zacharoulis S, Levy A, Chi SN, et al. Outcome for young children newly diagnosed with ependymoma, treated with intensive induction chemotherapy followed by myeloablative chemotherapy and autologous stem cell rescue. *Pediatr Blood Cancer*. 2007;49(1):34-40.
9. Farmer JP, Montes JL, Freeman CR, et al. Brainstem gliomas. A 10-year institutional review. *Pediatr Neurosurg*. 2001;34(4): 206-214.
10. Freeman CR, Farmer JP. Pediatric brain stem gliomas: a review. *Int J Radiat Oncol Biol Phys*. 1998;40(2):265-271.
11. Mandell LR, Kadota R, Freeman C, et al. There is no role for hyperfractionated radiotherapy in the management of children with newly diagnosed diffuse intrinsic brainstem tumors: results of a Pediatric Oncology Group phase III trial comparing conventional vs. hyperfractionated radiotherapy. *Int J Radiat Oncol Biol Phys*. 1999;43(5):959-964.
12. Pan E, Prados M. Brainstem gliomas. In: Gupta N, Haas-Kogen D, Banerjee A, eds. *Pediatric CNS Tumors*. Berlin, Heidelberg, New York: Springer-Verlag; 2004:49-61.
13. Nelson MD Jr, Soni D, Baram TZ. Necrosis in pontine gliomas: radiation induced or natural history? *Radiology*. 1994;191(1): 279-282.
14. Yoshimura J, Onda K, Tanaka R, et al. Clinicopathological study of diffuse type brainstem gliomas: analysis of 40 autopsy cases. *Neurol Med Chir (Tokyo)*. 2003;43(8):375-382; discussion 382.
15. Beaulieu C. The basis of anisotropic water diffusion in the nervous system—a technical review. *NMR Biomed*. 2002; 15(7-8):435-455.
16. Le Behan D, Mangin JF, Poupon C, et al. Diffusion tensor imaging: concepts and applications. *J Magn Reson Imaging*. 2001; 13(4):534-546.
17. Conturo TE, McKinstry RC, Akbudah E, Robinson BH. Encoding of anisotropic diffusion with tetrahedral gradients: a general mathematical diffusion formalism and experimental results. *Magn Reson Med*. 1996;35(3):399-412.
18. Basser PJ, Jones DK. Diffusion-tensor MRI: theory, experimental design and data analysis—a technical review. *NMR Biomed*. 2002;5(7-8):456-467.
19. Wimberger DM, Roberts TP, Barkovich AJ, Prayer LM, Moseley ME, Kucharczyk J. Identification of "premyelination" by diffusion-weighted MRI. *J Comput Assist Tomogr*. 1995; 19(1):23-33.
20. Prayer D, Barkovich AJ, Kirschner DA, et al. Visualization of nonstructural changes in early white matter development on diffusion-premyelination anisotropy. *AJNR Am Neuroradiol*. 2001;22(8):1572-1576.
21. Snimony JS, McKinstry RC, Akbudak E, et al. Quantitative diffusion-tensor anisotropy imaging: normative human data and anatomic analysis. *Radiology*. 1999;12(3):770-784.
22. Neil JJ, Shiran SI, McKinstry RC, et al. Normal brain in human newborns: apparent diffusion coefficient and diffusion anisotropy measured by using diffusion tensor MR imaging. *Radiology*. 1998;209(1):57-66.
23. Conturo TE, Lri NF, Cull TS, et al. Tracking neuronal fiber pathways in the living human brain. *Proc Natl Acad Sci U S A*. 1999;96(18):10422-10427.
24. Mori S, Crain BJ, Chacko VP, van Zijl PC. Three-dimensional tracking of axonal projections in the brain by magnetic resonance imaging. *Ann Neurol*. 1999;45(2):265-269.
25. Basser PJ, Pajevic S, Pierpaoli C, et al. In vivo fiber tractography using DT-MRI data. *Magn Reson Med*. 2000;44(4):625-632.
26. Barkovich AJ. *Pediatric Neuroimaging*. 4th ed. Philadelphia, PA: Lippincott; 2005.
27. Lien YH, Shapiro JI, Chan L. Effects of hypernatremia on organic brain osmoles. *J Clin Invest*. 1990;85(5):1427-1435.
28. Kreis R. Metabolic disorders of the brain in chronic hepatic encephalopathy detected with H-1 MR spectroscopy [see comments.]. *Radiology*. 1992;182(1):19-27.
29. Ball Jr WS, Holland SK. Pefusion imaging in the pediatric patient. *Magn Reson Imaging Clin N Am*. 2001;9(1):207-230.
30. Huisman TA, Sorenson AG. Perfusion-weighted magnetic resonance imaging of the brain: techniques and application in children. *Eur Radiol*. 2004;14(1):59-72.
31. Ostergaard L, Weisskoff RM, Chelser DA, et al. High-resolution measurement of cerebral blood flow using intravascular tracer bolus passages. Part I: Mathematical approach and statistical analysis. *Magn Reson Med*. 1996;36(5):715-725.
32. Detre JA, Aslop DC. Perfusion fMRI with areterial spin labeling based perfusion imaging techniques for MRI. In: Moonen CTW,

Bandetti PA, eds. *Fuctional MRI*. Heidelberg (Germany): Springer-Verlag; 1999:47-62.
33. Detre JA, Leigh JS, Williams DS, Koretsky AP. Perfusion imaging. *Magn Reson Med*. 1992;23(1):37-45.
34. Calamante F, Thomas Dl, Pell GS, Wiersma J, Turner R. Measuring cerebral blood flow using magnetic resonance imaging techniques. *J Cereb Blood Flow Metab*. 1999;19(7):701-735.
35. Wong EC, Buxton RB, Frank LR. Quantitative imaging of perfusion using a single subtraction (QUIPSS and QUIPSS II). *Magn Reson Med*. 1998;39(5):702-708.
36. Buxton RB, Frank LR, Wong EC, Siewert B, Warach S, Edelman RR. A general kinetic model for quatitative perfusion imaging with arterial spin labeling. *Magn Reson Med*. 1998;40(3):383-396.
37. Tanner SF, Cornette L, Ramenghi LA, et al. Cerebral perfusion in infants and neonates: preliminary results obtained using dynamic susceptibility contrast enhanced magnetic resonance imaging. *Arch Dis Child Fetal Neonatal Ed*. 2003;88(6):F525-F530.
38. Moreno-Torres A, Martinez-Perez I, Baquero M, et al. Taurine detection by proton magnetic resonance spectroscopy in medulloblastoma: contribution to noninvasive differential diagnosis with cerebellar astrocytomas. *Neurosurgery*. 2004;55(4):824-829.
39. Wilke M, Eidenschink A, Muller-Weihrich S, Auer DP. MR diffusion imaging and 1H spectroscopy in a child with medulloblastoma. A case report. *Acta Radiol*. 2001;42(1):39-42.
40. Tong Z, Yamaki T, Harada K, Houkin K. In vivo quantification of the metabolites in normal brain and brain tumors by proton MR spectroscopy using water as an internal standard. *Magn Reson Imaging*. 2004;22(7):1017-1024.
41. Kovanlikaya A, Panigrahy A, Krieger MD, et al. Untreated pediatric primitive neuroectodermal tumor in vivo: quantitation of taurine with MR spectroscopy. *Radiology*. 2005;236(3):1020-1025.
42. Rumboldt Z, Camacho DL, Lake D, Welsh CT, Castillo M. Apparent diffusion coefficients for differentiation of cerebellar tumors in children. *AJNR Am J Neuroradiol*. 2006;27(6):1362-1369.
43. Ball WS Jr, Holland SK. Perfusion imaging in the pediatric patient. *Magn Reson Imaging Clin N Am*. 2001;9(1):207-230, ix.
44. Cha S. Dynamic susceptibility-weighted contrast-enhanced perfusion MR imaging in pediatric patients. *Neuroimaging Clin N Am*. 2006;16(1):137-147, ix.
45. Panigrahy A, Krieger MD, Gonzalez-Gomez I, et al. Quantitative short echo time 1H-MR spectroscopy of untreated pediatric brain tumors: preoperative diagnosis and characterization. *AJNR Am J Neuroradiol*. 2006;27(3):560-572.
46. Albright AL, Packer RJ, Zimmerman R, Rorke LB, Boyett J, Hammond GD. Magnetic resonance scans should replace biopsies for the diagnosis of diffuse brain stem gliomas: a report from the Children's Cancer Group. *Neurosurgery*. 1993;33(6):1026-1029; discussion 1029-1030.
47. Jallo GI, Biser-Rohrbaugh A, Freed D. Brainstem gliomas. *Childs Nerv Syst*. 2004;20(3):143-153.
48. Barkovich AJ, Krischer J, Kun LE, et al. Brain stem gliomas: a classification system based on magnetic resonance imaging. *Pediatr Neurosurg*. 1990;16(2):73-83.
49. Seymour ZA, Panigrahy A, Finlay JL, Nelson MD Jr, Blüml S. Citrate in pediatric CNS tumors? *AJNR Am J Neuroradiol*. 2008;29(5):1006-1011.
50. Panigrahy A, Nelson MD Jr, Finlay JL, et al. Metabolism of diffuse intrinsic brainstem gliomas in children. *Neuro Oncol*. 2008;10(1):32-44.
51. Panigrahy A, Krieger M, Gonzalez-Gomez I, et al. Differentiation of encephalitis from astrocytomas in pediatric patients by quantitative in vivo MR spectroscopy. Paper presented at the 47th annual meeting of the American Society of Neuroradiology, in Chicago, Illinois, June 2007.
52. Central Brain Tumor Registry of the United States. *Statistical report: primary brain tumors in the United States, 1997-2001*. Author: 2004.
53. Karren EW. Molecularly targeted therapy for pediatric brain tumors. *J Neurooncol*. 2005;75(3):335-343.